buildings

Article

Simplified Procedure for Rapidly Estimating Inelastic Responses of Numerous High-Rise Buildings with Reinforced Concrete Shear Walls

Phichaya Suwansaya * and Pennung Warnitchai

Department of Civil and Infrastructure Engineering, Asian Institute of Technology, Pathum Thani 12120, Thailand
* Correspondence: phichaya.s@gmail.com

Abstract: Nonlinear response history analysis (NLRHA) is considered the most accurate procedure for evaluating the seismic performance of high-rise buildings. However, it requires considerable expertise and analysis time, making it inappropriate for some applications involving numerous high-rise buildings (e.g., the seismic loss estimation of a city). To overcome this limitation, a simplified procedure developed based on the uncoupled modal response history analysis (UMRHA) and coupled shear-flexural cantilever beam model (CSFCBM) is proposed. The underlying assumption is that the UMRHA procedure can compute the nonlinear seismic responses mode by mode, where each vibration mode is assumed to behave as a single-degree-of-freedom system. The nonlinear seismic responses are approximately represented by the sum of the modal responses of a few vibration modes. However, UMRHA requires knowledge of the modal properties and modal hysteretic behaviors. Therefore, the CSFCBM was introduced here to estimate the required modal properties and modal hysteretic behaviors. The inelastic seismic demands of the building can be determined using the UMRHA procedure with the computed modal properties obtained by CSFCBM. The accuracy of this proposed procedure was verified considering four high-rise buildings of 19, 30, 34, and 45 stories with reinforced concrete shear walls. The inelastic demands computed by the NLRHA procedure were used as a benchmark and compared with those of the proposed procedure. The results indicate that the proposed procedure provides reasonably accurate demand estimations for all case study buildings. Additionally, the total calculation time for modeling one building, performing dynamic analysis on 24 cases of ground motions, and post-processing the results required by the proposed procedure was about 7 to 45 times lower than that of the NLRHA procedure. Therefore, it can be used for estimating the seismic damage and losses of many high-rise buildings in a city for a specific earthquake scenario or a quick assessment of various seismic design options of a high-rise building in the preliminary design phase.

Keywords: high-rise buildings; nonlinear higher mode responses; modal hysteretic model; simplified procedure; seismic evaluation; RC shear walls

Citation: Suwansaya, P.; Warnitchai, P. Simplified Procedure for Rapidly Estimating Inelastic Responses of Numerous High-Rise Buildings with Reinforced Concrete Shear Walls. *Buildings* **2023**, *13*, 670. https://doi.org/10.3390/buildings13030670

Academic Editor: Nerio Tullini

Received: 20 January 2023
Revised: 26 February 2023
Accepted: 27 February 2023
Published: 2 March 2023

1. Introduction

In recent decades, the construction of high-rise buildings has significantly increased worldwide. Such buildings have become important elements of modern cities with a large city population living or working therein. Typically, high-rise buildings are constructed as reinforced concrete (RC) buildings, with RC slab-column frames or beam-column frames to carry gravity loads and RC shear walls to primarily resist lateral loads [1,2]. The safety and serviceability of these buildings against earthquakes are major concerns for the building residents, city officials, and other stakeholders [3]. However, evaluating the seismic safety and serviceability of such structures is difficult for several reasons. First, each building comprises various structural and non-structural components with different properties and response characteristics [4]. Second, its dynamic responses to seismic ground shaking are also considerably complicated, wherein several vibration modes other than the fundamental mode often contribute significantly to the responses [5]. Third, the responses to strong ground shakings that determine the seismic safety of the building are likely to exceed the elastic limits of the structure, causing various types of damage to different components of the building. Therefore, the methodology or analysis procedure selected for assessing the seismic performance (safety and serviceability) of the building must account for all these factors accurately.

In practice, the seismic performance of high-rise buildings is commonly evaluated using the nonlinear response history analysis (NLRHA) procedure [6]. It begins with the construction of a nonlinear finite element model (FEM) of the building, wherein the model comprises several hundreds or thousands of elements. The elements whose responses are expected to exceed the corresponding elastic limits must be modeled for their nonlinear load response behaviors. The construction of such a complex nonlinear model requires detailed information about the building components and advanced knowledge on their nonlinear structural behaviors, which is a time-consuming and laborious task. Subsequently, the nonlinear responses of the model to various input ground motions are computed by solving numerous coupled nonlinear differential equations. This step also requires significant amounts of computational resources and time. The computed results are obtained as the time histories of the element responses, which require further post-processing work to determine the maximum or minimum response values (seismic demands) and identify the corresponding damage state of the building. Therefore, the entire process may require several weeks or months to complete for a specific building.

The aforementioned seismic performance evaluation procedure may be suitable for certain applications, particularly when the accuracy and reliability of the evaluation results are crucial and only a few buildings are to be evaluated. For instance, the procedure can be used to check the design of a high-rise building in the final design stage to ensure that all seismic responses of interest are within acceptable limits [7]. It can also be used to guide the seismic retrofit design of existing high-rise buildings [6]. However, this procedure may not be suitable for other applications; for instance, the estimation of seismic losses of a city for an earthquake scenario requires a seismic performance evaluation of numerous high-rise buildings [8]. It is practically impossible to apply the NLRHA-based procedure to all the buildings. Moreover, detailed information on each building may not be available, making it unfeasible to construct nonlinear FEMs. Nevertheless, highly accurate seismic evaluation results may not be required in such cases, and reasonable accuracy can be acceptable.

In this study, a new simplified analysis procedure for evaluating the nonlinear seismic responses of numerous high-rise buildings with RC shear walls was proposed. It was developed from the use of the uncoupled modal response history analysis (UMRHA) procedure [9,10] and the coupled shear-flexural cantilever beam modal (CSFCBM) [11]. The UMRHA procedure facilitates the computation of nonlinear seismic responses mode by mode, where each vibration mode is assumed to behave as a nonlinear single-degree-of-freedom (SDOF) system. The nonlinear seismic responses are approximately represented by the sum of the modal responses of several vibration modes. The UMRHA procedure was applied to estimate the nonlinear seismic responses of several high-rise buildings with different heights, configurations, and arrangements of shear walls, and its accuracy was found to be satisfactory [12–14]. By this method, the degrees of freedom could be reduced from several thousands (NLRHA) to just a few (UMRHA), and the computational effort and time were significantly reduced. However, the UMRHA procedure requires knowledge of the modal properties and modal hysteretic behavior. These modal parameters can be obtained from an eigen analysis and a cyclic modal pushover analysis (MPA) of a complete three-dimensional (3D) nonlinear FEM. This is, as mentioned earlier, time- and effort-consuming work. Therefore, CSFCBM was introduced here to approximately represent high-rise buildings. CSFCBM is one of the simplest models that can simulate the complex behavior of a wall-frame structural system. The model is used to estimate the required modal properties and modal hysteretic parameters without constructing a complete 3D nonlinear FEM. Thus, the required information about the building will also be reduced to a bare minimum, facilitating the application of the proposed procedure to cases where detailed information of targeted buildings is unavailable.

The proposed simplified analysis procedure has several potential applications. It can be used for estimating the seismic damage and losses of many high-rise buildings in a city for a specific earthquake scenario. Risk-based premiums for earthquake insurance of high-rise buildings can also be determined based on the evaluation results obtained from this procedure. Additionally, it can be used for a quick assessment of various seismic design options of a high-rise building in the preliminary design phase, where many structural details are not yet specified, and an accurate estimate of seismic responses may not be required. Note that the proposed procedure can be modified to match the building information available. If detailed information is unavailable, the procedure can be adjusted such that it provides a reasonable estimate of seismic performance under such a data constraint. On the other hand, if detailed information is available, the procedure may be adjusted to obtain more accurate evaluation results. The theoretical framework of the proposed procedure and its application to selected case study buildings are presented in the subsequent sections.

2. UMRHA Procedure

Chopra and Goel [10] initially developed the UMRHA procedure, which was later simplified into the well-known MPA procedure. The UMRHA procedure can be considered an extended version of the conventional modal analysis procedure. In the latter, the complicated dynamic responses of an elastic multi-degree-of-freedom (MDOF) structure are represented by a sum of individual response from many vibration modes. The response of each mode is basically comparable to that of a single-degree-of-freedom (SDOF) system, which is governed by a few modal parameters making it is thus easy to handle. Furthermore, in most practical cases, it is sufficient to consider the first few modes to adequately represent the complicated structural responses. The conventional modal analysis procedure can be utilized to any elastic system.

The UMRHA procedure, which is based on the conventional modal analysis procedure, aims to extend the scope to inelastic structures. The theoretical basis of modal analysis is valid for linear systems; however, it is still assumed that it is approximately valid for inelastic systems. Therefore, vibration modes continue to exist even for inelastic responses, and complicated inelastic responses can be approximately described as a sum of these modal responses. The responses of a building in each vibration mode can be treated as that of a nonlinear single-degree-of-freedom system, where the governing equation of motion is given below:

$$\ddot{D}_i(t) + 2\xi_i\omega_i\dot{D}_i(t) + F_{si}\left(D_i, \dot{D}_i\right)/L_i = -\ddot{u}_g(t) \tag{1}$$

Herein, L_i is defined by $L_i = \Gamma_i M_i$ where Γ_i is the i^{th} modal participation factor and M_i is the i^{th} modal mass. ω_i is the i^{th} natural circular frequency, and ξ_i is the i^{th} damping ratio. $D_i(t)$ is the i^{th} mode response time history for any input ground motion, $\ddot{u}_g(t)$. More details about the derivation of UMRHA can be found in [10,13].

To compute the response time history of $D_i(t)$ from this equation, one needs to know the modal properties (ω_i, ξ_i, M_i, Γ_i) and modal restoring force F_{si}, which is a nonlinear function of D_i and $\dot{D}_i$. The latter defines the modal hysteretic response of a building.

A cyclic MPA is a direct technique to identify this complex modal hysteretic response of a building. This analysis is typically performed for each and every important vibration mode. For the i^{th} mode, the analysis is accomplished by first applying gravity loads, then applying lateral forces with the i^{th} modal inertia force pattern over the height of the building. The gravity loads are kept constant, whereas the magnitude of these lateral forces is gradually increased and reversed to produce cyclic responses with steadily increasing amplitude. Under this force pattern, the lateral displacements and other responses are anticipated to be dominated by those of the i^{th} mode. Having these responses, one can construct the cyclic relationship between the modal base shear, $V_i(0)$, and modal roof displacement, $u_i(H)$. This relationship can be transformed into the F_{si}–D_i relationship by assuming the deform shape at any point during the cyclic MPA corresponds to a natural vibration mode shape. Based on this assumption, the relationship between $u_i(H)$ and D_i can be determined using

$$D_i = \frac{u_i(H)}{\Gamma_i \phi_i(H)} \tag{2}$$

where $\phi_i(H)$ denotes the i^{th} natural vibration mode shape of the building at height H.

Under this force pattern, the relationship between $V_i(0)$ and F_{si} can be calculated as

$$\frac{F_{si}}{L_i} = \frac{V_i(0)}{\Gamma_i L_i} \tag{3}$$

An appropriate nonlinear hysteretic model can be chosen at this stage, and its properties can be modified to fit the F_{si}–D_i relationship. The response time history of a nonlinear SDOF system ($D_i(t)$ and $F_{si}(t)$) can then be determined using Equation (1). $D_i(t)$ is used to determine all deformation-related responses, including lateral floor displacements and interstory drift ratios of the i^{th} mode, whereas $F_{si}(t)$ is used to compute all force-related responses, including story shears and overturning moments of the i^{th} mode. For example, the lateral floor displacement of the i^{th} mode can be determined as follows:

$$u_i(x,t) = \Gamma_i \phi_i(x) D_i(t) \tag{4}$$

where $u_i(x,\ t)$ indicates the lateral floor displacement contributed by the i^{th} mode, and $\phi_i(x)$ denotes the i^{th} natural vibration mode shape at a particular height x above the building's base. The interstory drift ratios can be easily calculated after determining the lateral floor displacements. The modal base shear, $V_i(0,\ t)$, is determined using Equation (3), whereas the modal base overturning moment ($OM_i(0,\ t)$), is calculated using the following equation:

$$OM_i(0,t) = \frac{F_{si}(t)}{L_i} \Gamma_i \sum_{j=1}^{N} x_j m_j \phi_i(x_j) \tag{5}$$

where x_j denotes the elevation of the j^{th} floor, M_j indicates the story mass of the j^{th} floor, and N represents the total number of floors. The relationships in Equations (4) and (5) are the results of the modal inertia force distribution pattern. For other force-related responses, their relationship with F_{si} can be obtained from MPA in the linear response range.

The force-related or deformation-related responses contributed by the i^{th} mode can be commonly expressed as $r_i(t)$. By summing the response histories of all the significant modes, the total response $r(t)$ is obtained as follows:

$$r(t) = \sum_{i=1}^{m} r_i(t) \tag{6}$$

where m denotes the number of significant vibration modes.

The theoretical concepts of the UMRHA procedure described in this section can be easily applied to many other types of structures. Compared with NLRHA, wherein the seismic responses are calculated by solving numerous coupled nonlinear differential equations, UMRHA requires only the solutions of "m" uncoupled nonlinear differential equations (Equation (1)). In most cases, the number of significant vibration modes, m, is as low as three to six [13,14]. Therefore, the computational time and resources required to compute the seismic responses are extremely low in the UMRHA procedure compared with those of the NLRHA procedure.

However, the formulation of "*m*" uncoupled nonlinear differential equations requires knowledge of the nonlinear modal restoring force $F_{si}\left(D_i,\ \dot{D}_i\right)$ and modal properties. If one constructs a nonlinear FEM of the building, the former can be obtained from a cyclic MPA, as explained earlier, and the latter can be obtained using eigen analysis of a linearized version of the model. All these nonlinear FEM constructions and associated analyses require a substantial amount of time and effort and detailed information about the building. Therefore, Section 3 introduces CSFCBM to represent the building. As the model allows the determination of the required modal properties and the nonlinear modal restoring force without the use of nonlinear FEMs, the seismic performance analysis process can be significantly simplified, and the required building information can be reduced to a bare minimum.

3. CSFCBM

Figure 1 depicts CSFCBM as an approximate model of a high-rise building with a frame-wall system. It may not be applicable to other structural systems (e.g., outrigger and belt truss). The model comprises a vertical cantilever flexural beam connected to a vertical cantilever shear beam by numerous axially rigid links that transmit only horizontal forces. Owing to this arrangement, the lateral deflections of the two beams remain identical when a lateral load is applied. The flexural beam represents the combined effects of RC walls and other structural components that deform in the flexural mode, whereas the shear beam represents the combined effects of frames and other structural components that deform in the shear mode. The links represent the slabs that horizontally connect RC walls and frames; the links are treated as rigid members because of the extremely high in-plane stiffness of the slabs.

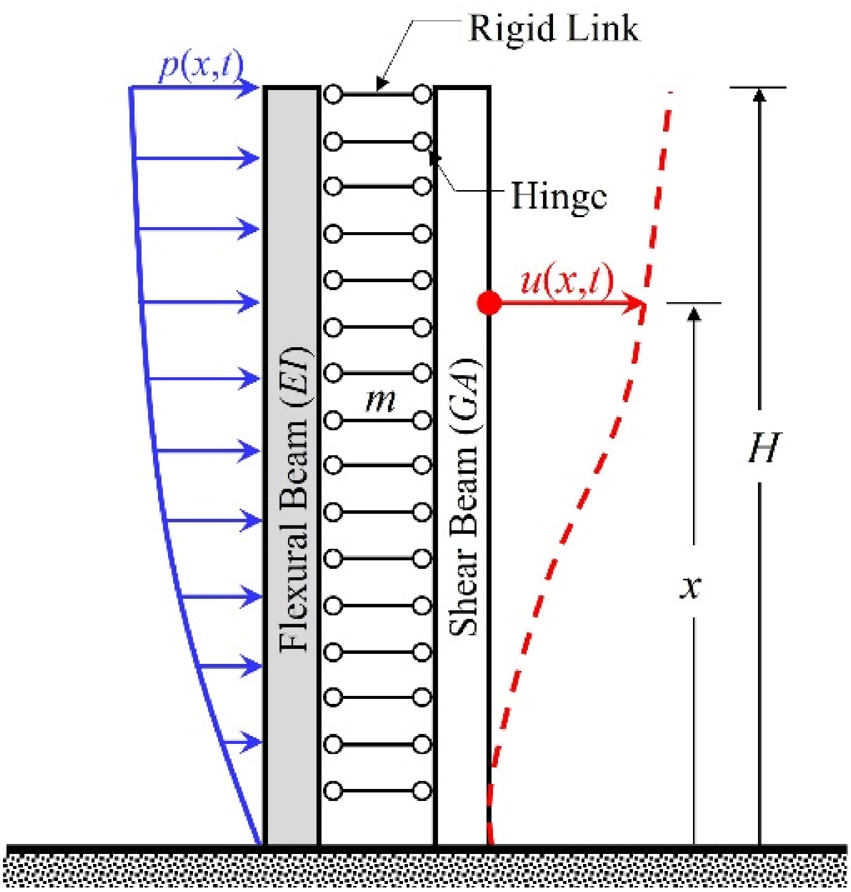

Figure 1. Definitions and properties of CSFCBM.

CSFCBM was first proposed by Khan and Sbarounis [15] to evaluate the interaction between walls and frames in multi-story buildings. The model was later used to identify approximate responses of multi-story buildings, such as lateral displacements and shear forces in walls, under various lateral load distributions [16–18]. Several closed-form formulas for predicting responses (e.g., lateral displacements) to certain lateral loading patterns have been derived from this model, and they are found to be sufficiently accurate when applied to 30- and 20-story case study buildings [18,19].

For earthquake excitation, Miranda [20] used CSFCBM to estimate the maximum roof displacement and maximum interstory drift ratio of multi-story buildings that primarily respond in the first mode of vibration. The estimated responses for a 10-story steel moment-resisting frame building concur well with those predicted by the detailed FEM. CSFCBM was further extended by Miranda and Reyes [21] to non-uniform lateral stiffness cases, where the flexural rigidity (EI) and shear rigidity (GA) were reduced along the height. However, they determined that the stiffness reduction does not exhibit a significant effect on the maximum interstory drift ratio demand, provided that no abrupt stiffness reductions occur in the structure.

Miranda and Taghavi [22] used CSFCBM to derive closed-form solutions for the vibration mode shapes, natural periods, and modal participation factors of multi-story buildings with uniform properties along their heights. They also extended their study to non-uniform lateral stiffness cases and determined that the stiffness reduction with increasing height does not have significant effects on the dynamic characteristics of the structure, particularly when the flexural action dominates the shear action. Miranda and Taghavi's [22] closed-form solutions were adopted by Reinoso and Miranda [23] for estimating the floor acceleration demands in high-rise buildings subjected to earthquake excitation. The estimated demand matched the actual acceleration records reasonably well. Subsequently, several other studies demonstrated the ability of CSFCBM to accurately estimate the linear elastic multi-mode responses of high-rise buildings under earthquake excitations [24,25].

Herein, we describe CSFCBM and the closed-form solutions for its modal properties derived by Miranda and Taghavi [22]. Several useful relationships from the CSFCBM are also derived and explained. These relationships were used for mapping the model to a specific high-rise building and constructing its nonlinear modal force $F_{si}\left(D_i,\ \dot{D}_i\right)$.

Based on the model presented in Figure 1, the governing equation of motion of the structure under the lateral-distributed force $p(x, t)$ is given by

$$m\frac{\partial^2 u(x,t)}{\partial t^2} + EI\frac{\partial^4 u(x,t)}{\partial x^4} - GA\frac{\partial^2 u(x,t)}{\partial x^2} = p(x,t) \tag{7}$$

where $u(x, t)$ denotes the lateral displacement at height x above the ground and time t, m indicates the mass per unit height of the building, EI represents the effective flexural rigidity of the flexural beam, and GA indicates the effective shear rigidity of the shear beam. This equation applies for $0 < x < H$, where H denotes the total height of the building. The lateral-distributed force $p(x, t)$ can be a wind-induced force, inertia force induced by earthquake shaking, or any other lateral loads.

At the fixed end ($x = 0$), the boundary conditions are

$$u(x,t)_{x=0} = 0 \text{ and } \left.\frac{\partial u(x,t)}{\partial x}\right|_{x=0} = 0 \tag{8}$$

At the free end ($x = H$), the boundary conditions are

$$\left.EI\frac{\partial^2 u(x,t)}{\partial x^2}\right|_{x=H} = 0 \text{and } \left.\left(EI\frac{\partial^3 u(x,t)}{\partial x^3} - GA\frac{\partial u(x,t)}{\partial x}\right)\right|_{x=H} = 0 \tag{9}$$

The free vibration analysis can be performed by setting $p(x, t)$ to zero in Equation (7), and the following modal properties of the CSFCBM can be obtained:

$$\omega_i = \gamma_i \sqrt{\alpha^2 + \gamma_i^2} \sqrt{\frac{EI}{mH^4}} \tag{10}$$

where ω_i denotes the natural circular frequency for the i^{th} vibration mode ($i = 1, 2, 3 \ldots$), and α is a non-dimensional parameter of the structure, which can be defined as

$$\alpha = H\sqrt{\frac{GA}{EI}} \tag{11}$$

Parameter γ_i indicates the eigenvalue parameter of the i^{th} vibration mode, which is obtained as the i^{th} solution of the following characteristic equation:

$$2 + \left(2 + \frac{\alpha^4}{\gamma_i^2(\alpha^2 + \gamma_i^2)}\right) \cos(\gamma_i) \cosh\left(\sqrt{\alpha^2 + \gamma_i^2}\right) + \left(\frac{\alpha^2}{\gamma_i\sqrt{\alpha^2 + \gamma_i^2}}\right) \sin(\gamma_i) \sinh\left(\sqrt{\alpha^2 + \gamma_i^2}\right) = 0 \tag{12}$$

The corresponding i^{th} vibration mode shape (ϕ_i) of the structure is given by

$$\phi_i(x) = \sin\left(\gamma_i \frac{x}{H}\right) - \frac{\gamma_i}{\sqrt{\alpha^2 + \gamma_i^2}} \sinh\left(\sqrt{\alpha^2 + \gamma_i^2}\frac{x}{H}\right) - \eta_i \cos\left(\gamma_i \frac{x}{H}\right) + \eta_i \cosh\left(\sqrt{\alpha^2 + \gamma_i^2}\frac{x}{H}\right) \tag{13}$$

where

$$\eta_i = \frac{\gamma_i^2 \sin(\gamma_i) + \gamma_i\sqrt{\alpha^2 + \gamma_i^2} \sinh\left(\sqrt{\alpha^2 + \gamma_i^2}\right)}{\gamma_i^2 \cos(\gamma_i) + \left(\alpha^2 + \gamma_i^2\right) \cosh\left(\sqrt{\alpha^2 + \gamma_i^2}\right)} \tag{14}$$

Based on the closed-form solution for the i^{th} vibration mode shape, several associated modal parameters (L_i, M_i, and Γ_i) can be determined as follows:

$$L_i = \int_0^H m\phi_i(x)dx,\ M_i = \int_0^H m\phi_i^2(x)dx, \text{ and } \Gamma_i = L_i/M_i \tag{15}$$

It is evident that the α parameter is instrumental in determining the modal characteristics of a building. For instance, the flexural action dominates when α is low (e.g., less than 1.0), and the shear action dominates when α is high (e.g., more than 10). Once α is specified, the eigenvalue parameter (γ_i) can be determined using the characteristic equation, and the corresponding mode shape (ϕ_i), modal frequency (ω_i), and natural period (T_i) can be obtained ($T_i = 2\pi/\omega_i$).

Furthermore, the i^{th} period ratio, defined as the ratio of the first-mode natural period (T_1) to the i^{th} mode natural period (T_i), also relies on α.

$$\frac{T_1}{T_i} = \frac{\gamma_i}{\gamma_1}\sqrt{\frac{\alpha^2 + \gamma_i^2}{\alpha^2 + \gamma_1^2}} \tag{16}$$

Figure 2 illustrates the second and third period ratios (T_1/T_2 and T_1/T_3) plotted against α. The vibration mode shapes of the first three modes for α = 0 and 100 are also depicted in the figure. In zone A, where α is less than 1.0, the period ratios T_1/T_2 and T_1/T_3 are relatively high, approaching 6.26 and 17.52, respectively, as α decreases to 0. These period ratio values are those of an ideal cantilever flexural beam. The corresponding vibration mode shapes in this zone are similar to those of α = 0 shown on the left-hand side of Figure 2. Conversely, in zone C, where α is greater than 10, the period ratios T_1/T_2 and T_1/T_3 are relatively low and approaching 3.0 and 5.0, respectively, as α increases to 100. These period ratio values are those of an ideal cantilever shear beam. The corresponding vibration mode shapes in zone C are similar to those of α = 100, as shown on the right-hand side of Figure 2.

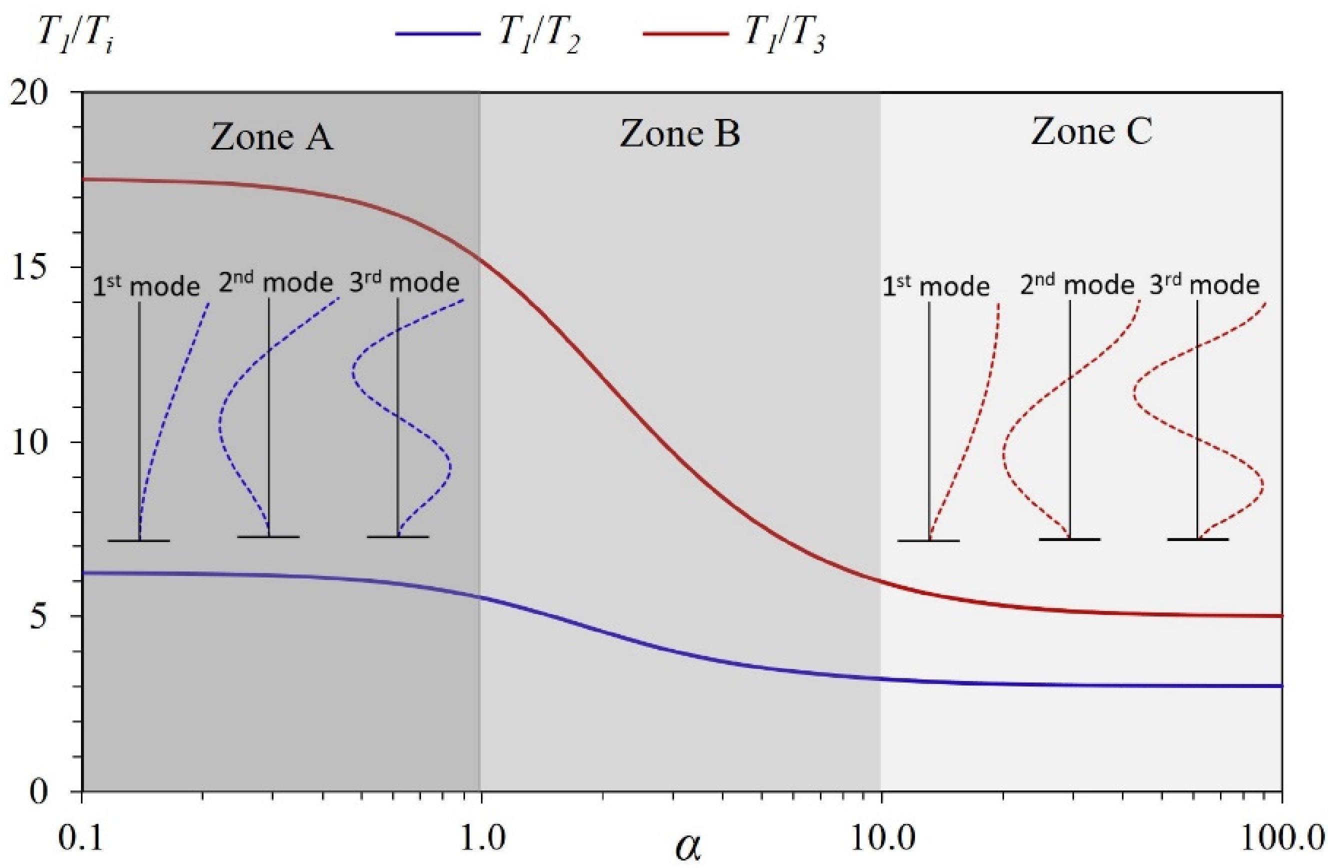

Figure 2. Effect of α on the period ratios of CSFCBM.

The α values of typical buildings are likely to be somewhere between these two extremes, namely, ideal flexural and shear beams. Their α values typically fall into zone B ($1 < \alpha < 10$), where the period ratios vary significantly with the change in α. This suggests that one could easily identify the α value of a given building by simply checking its period ratios.

To represent a high-rise building using CSFCBM, one needs to determine the model parameters, namely, H, M, EI, and GA. Among these, height H is a basic building parameter that can be obtained easily. The mass per unit height m can also be estimated conveniently if the detailed drawings of the building are available. Otherwise, m can be approximately estimated from the gross mass density (ρ_b) of buildings in the same class. The gross mass density is defined as the total building mass divided by the total encased volume of the building. The gross mass density of RC buildings, for example, typically varies from 250 to 350 kg/m^3. However, the remaining two parameters, EI and GA, are difficult to evaluate directly despite the availability of detailed drawings [18]. Section 4 discusses this further, where the case study buildings are examined.

Based on the relationships explained in this section, it is possible to estimate the values of EI and GA if the first- and second-mode periods (T_1, T_2) of the building are known. Initially, the value of α can be determined from the period ratio T_1/T_2 using Equations (16) and (12). Subsequently, EI can be determined from T_1 using Equation (10), and GA can be calculated using the known values of EI and α. Alternatively, the values of EI and GA can be estimated if T_1 and α are known.

Several empirical formulas are available for estimating the T_1 of high-rise buildings. For instance, an empirical formula $T_1 = 0.019H$ is provided in the seismic design standard of Thailand, which was derived from the ambient vibration measurement data of numerous existing RC buildings in the country [26]. Based on these vibration measurements, it is also possible to obtain the period ratio T_1/T_2 or, in some cases, T_1/T_3 to identify the value of α [27]. Nevertheless, if some details of RC walls and frames of the building are available, one may calculate a certain structural index and use it for estimating the value of α; further details are presented in Section 4. Alternatively, if a linear elastic FEM of the building is available, the first- and second-mode periods (T_1, T_2) can be obtained using a standard eigen analysis.

In summary, the CSFCBM of a specific high-rise building can be determined through multiple alternative methods. The choice of method may rely on the available building information. Once the CSFCBM is determined, the necessary modal properties of the building can be readily evaluated using Equations (10)–(15). However, the evaluation of the nonlinear modal restoring force $F_{si}\left(D_i,\ \dot{D}_i\right)$ requires further analysis. The subsequent sections present certain important relationships for this evaluation.

Considering that the building vibrates in its i^{th} mode, that is, $u(x,t) = u_i(x,t) = \phi_i(x)q(t) = \Gamma_i\phi_i(x)D_i(t)$, the shear forces in the flexural beam ($V_i^F(x,\ t)$) and shear beam ($V_i^s(x,\ t)$) are given by

$$V_i^f(x,t) = -EI\frac{\partial^3 u(x,t)}{\partial x^3} = -EI\Gamma_i\phi_i{}'''(x)D_i(t) \tag{17}$$

$$V_i^s(x,t) = GA\frac{\partial u(x,t)}{\partial x} = GA\Gamma_i\phi_i{}'(x)D_i(t) \tag{18}$$

The shear force $V_i^F(x,\ t)$ is approximately equal to the sum of the shear forces in all RC walls in that story, whereas $V_i^s(x,\ t)$ is approximately equal to the sum of the shear forces in all frames. The sum of $V_i^F(x,\ t)$ and $V_i^s(x,\ t)$ is equal to the story shear, denoted as $V_i^t(x,\ t)$. Note that the superscript is denoted as the responses obtained by CSFCBM.

Similarly, the overturning moments in the flexural beam ($OM_i^F(x,\ t)$) and shear beam ($OM_i^s(x,\ t)$) are given by

$$OM_i^f(x,t) = \int_x^H V_i^f(x,t)dx = -EI\Gamma_i D_i(t)\int_x^H \phi_i{}'''(x)dx \tag{19}$$

$$OM_i^s(x,t) = \int_x^H V_i^s(x,t)dx = GA\Gamma_i D_i(t)\int_x^H \phi_i{}'(x)dx \tag{20}$$

Here $OM_i^F(x,\ t)$ is approximately equal to the sum of the overturning moments contributed by all RC walls, and $OM_i^s(x,\ t)$ is approximately equal to the sum of the overturning moments contributed by all frames. The sum of $OM_i^F(x,\ t)$ and $OM_i^s(x,\ t)$ is equal to the story overturning moment, denoted as $OM_i^t(x,\ t)$.

Therefore, the separate contributions of RC walls and frames to the story shear and story overturning moment of the building can be determined based on the aforementioned relationships.

In the case of a building with well-isolated RC walls, the bending curvature ($\varphi_i(x,\ t)$) of each individual wall is identical and given as

$$\varphi_i(x,t) = \frac{\partial^2 u(x,t)}{\partial x^2} = \Gamma_i\phi_i{}''(x)D_i(t) \tag{21}$$

The corresponding flexural strain at the extreme tension face (fiber) of any RC wall can be calculated as

$$\varepsilon_{i,f}(x,t) = |\varphi_i(x,t)|L_t = |\Gamma_i\phi_i{}''(x)D_i(t)|L_t \tag{22}$$

where L_t denotes the distance measured from the neutral axis of the cross-section of the wall to the extreme tension face (fiber) of the wall. Note that if the distance from the neutral axis to the extreme compression face of the wall (L_c) is substituted with L_t in Equation (22), the corresponding flexural strain at the extreme compression face can also be computed.

This flexural strain can later be used to determine the flexural tensile cracks and yielding of the rebars that occur in the wall. All these relationships are essential for deriving the modal hysteretic response of a high-rise building. The derivation process is explained in detail in Section 5.

4. Case Study Buildings

The four high-rise buildings chosen for the case study had heights ranging from 19 to 45 stories and were located in Bangkok, Thailand. They were used as reference cases to verify the accuracy of CSFCBM in estimating the building modal properties and evaluating the building seismic responses. These buildings were named S1, B1, B2, and B3, and their typical floor plans and 3D views are depicted in Figure 3. In every building, the gravity-load-carrying and lateral-load-resisting components were RC slab-column frames (gray and blue regions) and RC walls or cores (red regions), respectively. Masonry infill walls (black dashed lines) were broadly used as exterior and interior partition walls. In all cases, the foundation structure was a mat foundation lying on piles. Buildings B1, B2, and B3 had podiums, and B1 had an unsymmetrical arrangement of RC walls in its tower floor plan; these are vertical and plan irregularities commonly found in high-rise buildings. Conversely, building S1 was a regular building with a symmetrical arrangement of RC walls and uniform structural properties along its height from the base to the top. Table 1 lists the key properties and characteristics of these buildings.

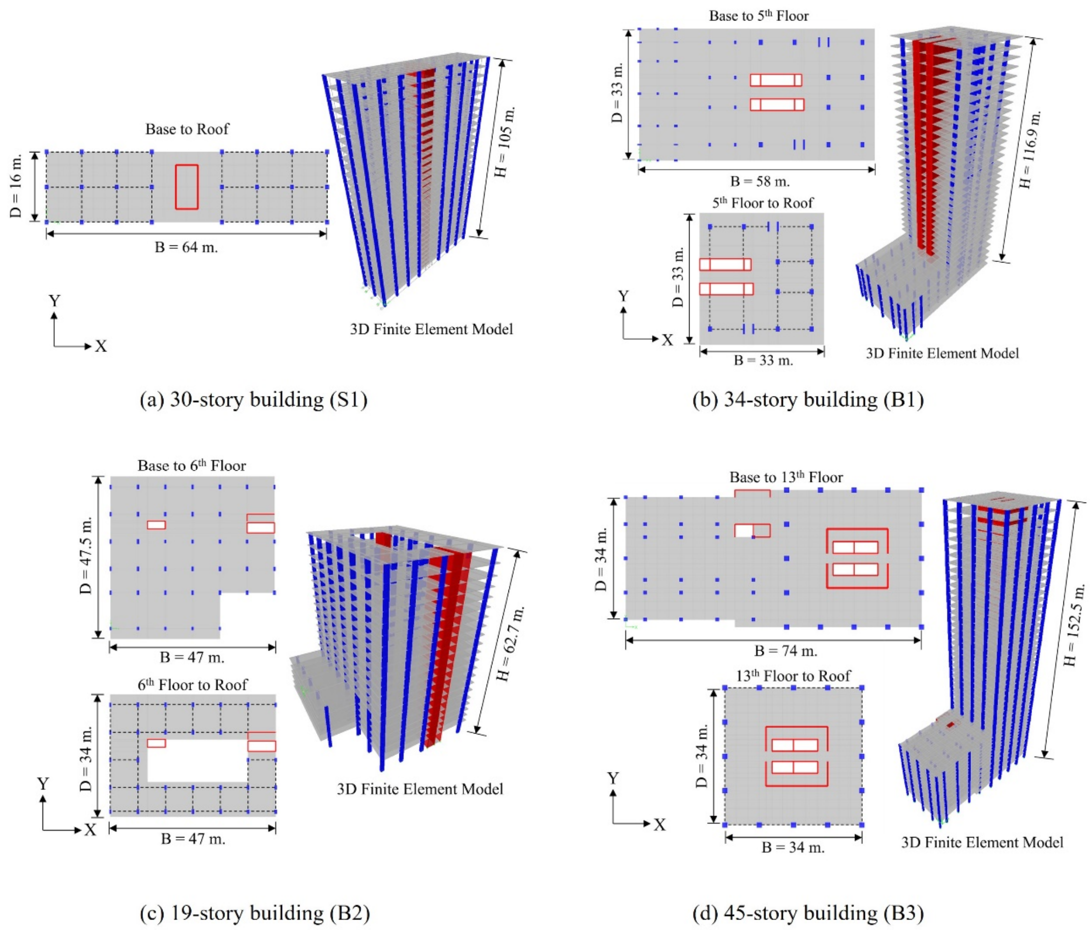

Figure 3. Typical floor plans and 3D views of the four case study buildings.

Table 1. Key properties and characteristics of four case study buildings.

Building Name		S1	B1	B2	B3
Width of the tower, B (m)		64.0	31.0	47.0	33.6
Depth of the tower, D (m)		16.0	32.5	34.0	33.6
Height, H (m)		105.0	116.9	59.5	152.5
No. of stories		30	34	19	45
Typical story height, h (m)		3.5	3.2	2.9	3.5
RC wall section area/footprint area (%)		0.88	1.62	0.54	2.42
RC column section area/footprint area (%)		2.81	1.45	1.06	2.04
RC typical wall thickness (m)	Base–10th floor	0.35	0.25	0.25	0.45
	10th–20th floor	0.35	0.25	0.25	0.40
	20th floor–roof	0.35	0.25	0.25	0.35
RC column typical dimension (m)	Base–10th floor	1.0 × 1.2	0.9 × 1.2	0.5 × 1.2	1.2 × 1.2
	10th–20th floor	1.0 × 1.2	0.9 × 1.2	0.5 × 1.2	1.2 × 1.2
	20th floor–roof	1.0 × 1.2	0.9 × 1.2	0.5 × 1.2	1.2 × 1.2
Longitudinal reinforcement ratio in RC wall (%)	Base–10th floor	4.0	1.27	2.27	2.95
	10th–20th floor	4.0	0.81	1.45	1.44
	20th floor–roof	4.0	0.46	0.93	1.44
Specified compressive strength of concrete, $f_c{}'$ (MPa)	RC walls	45	45	42	45
	RC column	45	32	42	40
	RC and PT slabs *	32	32	32	32
Specified yield strength of longitudinal reinforcement steel bar, f_y (MPa)		490	390	390	390

* PT slabs = post-tensioned concrete slabs.

4.1. FEM of Case Study Building

Perform 3D version 7 [28] was used to create nonlinear FEMs of the four buildings. The models were utilized to determine the buildings' modal hysteretic behavior using cyclic MPA and to compute their nonlinear seismic responses. Linearized versions of these models (linear FEMs) were used to determine the modal properties of these buildings.

Nonlinear fiber elements were used to model each RC wall throughout its height since flexural cracking and yielding may form at any level. To simulate the combined axial and flexural behaviors of the wall, it was divided into numerous horizontal layers, each of which comprise numerous vertical concrete and steel fibers. The term "multi-vertical-line-element model" (MVLEM) is used to describe this kind of model [29,30]. Additionally, each layer also has a horizontal elastic shear spring to account for shear response. For the steel fibers, a bilinear hysteretic model of the non-degrading type with 1.25% post-yield stiffness was used. As the actual material strength is typically greater than the nominal value, the actual yield strength of steel rebars was set to be 1.17 times its nominal yield strength (Table 1), as recommended by LATBSDC [31] and TBI [3]. Similarly, the actual cylinder compressive strength of concrete ($f_c{}'$) was assumed to be 1.3 times the nominal strength [3,31]. When fabricating concrete fibers, Mander's stress–strain model [32] was used for either confined or unconfined concrete, and it was approximated by a trilinear envelope. In Peform3D, although the unloading stiffness of the concrete hysteretic model is inherently set equal to the initial elastic stiffness, the reloading stiffness can be tuned in such the way that it decreases with an increase in the plastic strain. The tensile strength of concrete was assumed to be 0.1 $f_c{}'$ MPa [33]. When the nonlinear FEM was linearized, the axial stiffness of the fibers was set equal to their initial low-stress stiffness value, which was approximately 1.5 times the stiffness computed using the ACI318 secant concrete modulus ($E_c = 4700\sqrt{f_c{}'}$).

For slab-column frames, every RC column was modeled by combining a linear elastic beam-column element with nonlinear plastic zones at its upper and lower ends in each story. The gross (uncracked) flexural rigidity was assigned to a linear element. The lengths of the plastic zones were set equal to those of the plastic hinges, as determined by the formula proposed by Paulay and Priestley [34]. These plastic zones were composed of numerous concrete and steel fibers in a manner similar to that of RC walls; this ensured that all states of the column, including cracking, yielding, and failure, were completely simulated. Concrete slabs, on the other hand, were assumed to be elastic and thus modeled using linear elastic thin-shell elements. The gross bending rigidity of E_cI_g and gross axial stiffness of E_cA_g were assigned to these slabs.

Although masonry infill walls are generally considered non-structural components, and their contributions to the stiffness and strength of the building system might be less than those of RC walls and frames, they were explicitly modeled in this study. Each infill wall was idealized with two compression-only inclined struts arranged in an X pattern. Their inelastic force–deformation relationship was defined by a trilinear envelope, and the hysteretic model was assumed to be similar to those described previously for concrete fibers. The wall cracking strengths and associated story drift angles were estimated using formulas proposed by Kappos et al. [35], and their ultimate strength was estimated using the formula recommended by MSJC [36]; further details can be found in Suwansaya [33]. When the seismic response time history is evaluated using these compression-only struts, only one strut in a wall panel is active at any time instant. However, when the nonlinear model is linearized, the combined stiffness of the two inclined struts from each wall panel is counted in the stiffness matrix of the building. Therefore, before performing the linearization, the axial stiffness of every strut was reduced by half to obtain a correct stiffness contribution.

The modal damping ratios were taken as 2.5% for every translational vibration mode based on the recommendations of TBI [3] and LATBSDC [31]. As the soil-foundation system was assumed to be substantially stiffer than that of the superstructure, the soil–structure interaction effects were neglected. Therefore, the mat foundation was considered a rigid boundary, which was horizontally displaced by the input ground motion.

4.2. Accuracy of CSFCBM in Estimating the Modal Properties and Responses

Buildings S1 and B1 were selected as reference cases to verify the accuracy of CSFCBM in estimating the vibration modal properties and modal responses. Building S1 represented regular high-rise buildings with symmetrical floor plans and uniform stiffness and mass along the height, whereas building B1 represented typical high-rise buildings with podium and non-symmetrical floor plans. The modal properties of the two buildings were first determined by an eigen analysis of their linearized FEMs and are summarized in Tables 2 and 3. Two CSFCBMs were created for each building, one for the motion along the x axis and the other for the y axis. Each model was created from four basic building parameters, namely, H, m, T_1, and T_2. The building height H is listed in Table 1. The mass per unit height m was estimated using the as-built drawings of the building. The natural periods T_1 and T_2 were computed using the linearized FEM. The parameters α, EI, and GA were determined using the procedure explained in Section 3; thus, CSFCBM was defined completely. The natural periods (T_i), mode shape (ϕ_i), modal mass (M_i), and modal participation factor (Γ_i) of the first three transverse vibration modes of CSFCBM could be obtained using Equations (10)–(15). These modal properties, along with the α parameter, are listed in Tables 2 and 3. Herein, the modal mass was normalized by the total mass of the building (M_t). We observed that the modal properties of CSFCBM concurred well with those of FEM for both buildings in both the X and Y directions. The differences were extremely low in the first mode and generally increased with an increase in the modal number.

Based on CSFCBM, various responses of each individual vibration mode can be easily estimated using the closed-form formulas. As all types of responses of the i^{th} mode in the linear elastic range are proportional to the modal coordinate $D_i(t)$, their response values for $D_i(t)$ of 0.001 m (1 mm) were evaluated. The lateral displacement of the i^{th} mode was determined by $u_i(x,\ t) = \Gamma_i\phi_i(x)D_i(t)$, where $D_i(t)$ = 0.001 m. The corresponding interstory drift ratio was obtained by considering the partial derivative of the displacement with respect to height x ($\Gamma_i\phi_i{}'(x)D_i(t)$), and the corresponding deformation curvature was determined using Equation (21). The deformation responses in the x direction of the first, second, and third modes are represented by the blue, red, and black dashed lines in Figure 4, respectively. The corresponding shear forces in the flexural and shear beams, namely, $V_i^f(x,\ t)$ and $V_i^s(x,\ t)$, were determined using Equations (17) and (18) and are represented by the blue and red dashed lines, respectively, in Figures 5 and 6. The sum of these shear forces is the story shear, $V_i^t(x,\ t)$, which is represented by the black dashed line. Similarly, the overturning moments in the flexural and shear beams, $OM_i^f(x,\ t)$ and $OM_i^s(x,\ t)$, were determined using Equations (19) and (20) and are represented by the blue and red dashed lines, respectively, in Figures 5 and 6. The sum of these moments is the story overturning moment $OM_i^t(x,\ t)$ and is represented by the black dashed line.

Table 2. Modal properties of building S1.

Modal Properties		X Direction FEM	X Direction CSFCBM	X Direction Error (%)	Y Direction FEM	Y Direction CSFCBM	Y Direction Error (%)
T_i (s)	First mode	4.420	4.420	-	3.371	3.371	-
	Second mode	1.088	1.089	-	0.744	0.745	-
	Third mode	0.477	0.447	6.4	0.322	0.289	10.3
M_i/M_T	First mode	0.677	0.666	1.6	0.657	0.647	1.6
	Second mode	0.162	0.143	11.8	0.184	0.159	13.5
	Third mode	0.063	0.059	6.0	0.065	0.062	5.1
Γ_i	First mode	1.465	1.477	0.8	1.503	1.514	0.7
	Second mode	−0.724	−0.767	6.1	−0.757	−0.810	7.0
	Third mode	0.414	0.495	19.5	0.411	0.502	22.0
T_1/T_2			4.063			4.531	
A			2.88			2.06	

Table 3. Modal properties of building B1.

Modal Properties		X Direction FEM	X Direction CSFCBM	X Direction Error (%)	Y Direction FEM	Y Direction CSFCBM	Y Direction Error (%)
T_i (s)	First mode	3.112	3.112	-	5.487	5.487	-
	Second mode	0.613	0.613	-	1.457	1.457	-
	Third mode	0.263	0.229	13.0	0.676	0.634	6.3
M_i/M_T	First mode	0.597	0.631	5.8	0.649	0.685	5.6
	Second mode	0.200	0.172	14.0	0.135	0.129	4.6
	Third mode	0.085	0.063	25.6	0.059	0.056	4.7
Γ_i	First mode	1.525	1.539	0.9	1.435	1.438	0.2
	Second mode	−0.814	−0.838	3.0	−0.689	−0.721	4.6
	Third mode	0.490	0.506	3.2	0.429	0.485	13.0
T_1/T_2			5.077			3.766	
A			1.43			3.76	

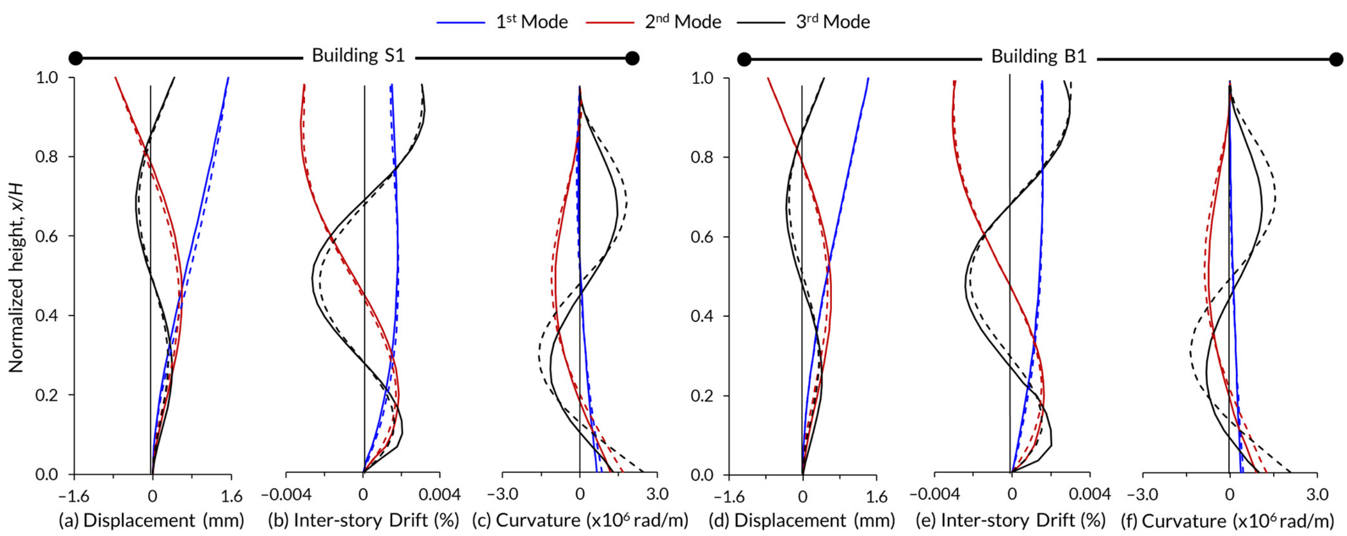

Figure 4. Deformation responses of buildings S1 and B1 in the x direction.

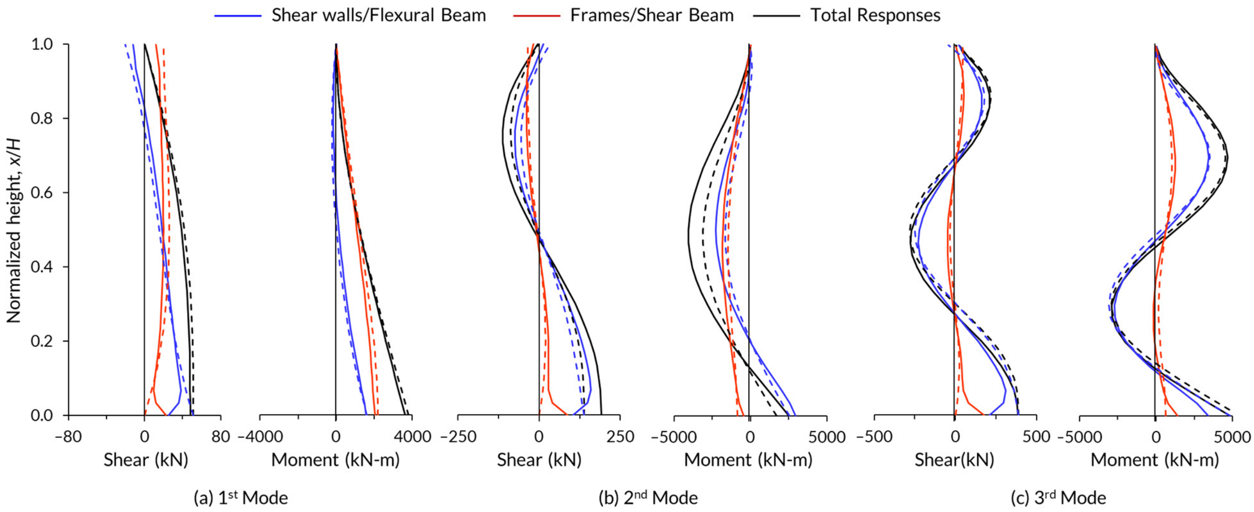

Figure 5. Force responses of building S1 in the x direction.

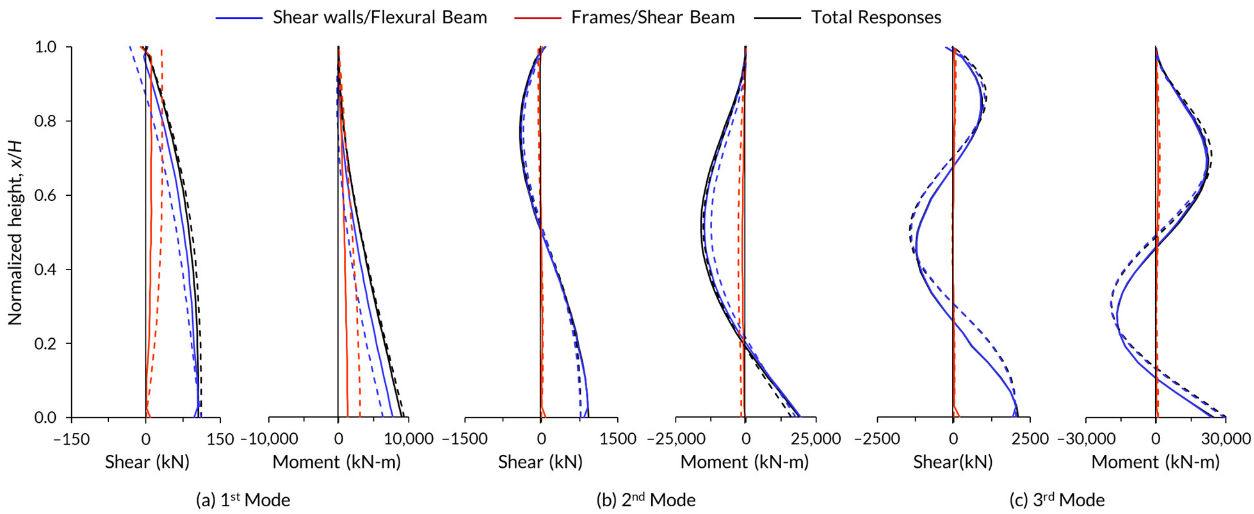

Figure 6. Force responses of building B1 in the x direction.

The accuracy of CSFCBM in estimating these various modal responses was verified by comparing their predictions with those computed from the linearized FEMs. The modal responses of the i^{th} mode were obtained by first applying the gravity loads and then applying lateral forces with the i^{th} modal inertia force pattern to the FEM of the building (i.e., modal pushover analysis). The lateral forces were scaled such that the lateral displacement at the building top ($x = H$) was exactly equal to that predicted by the CSFCBM. The corresponding lateral displacements at other floors were obtained in a straightforward manner; all these displacements were determined at the geometric center of the tower's plan section. The corresponding interstory drift ratio at any height was computed from the difference in lateral displacements of the floors above and below that height. The corresponding deformation curvature was computed from the difference in the vertical strains at two opposite extreme fibers of the RC walls. All modal deformation responses computed by the FEM are plotted in Figure 4 by blue, red, and black lines for the first, second, and third modes, respectively. These modal deformation responses concurred well with those predicted by CSFCBM, confirming its accuracy in this aspect. Although the differences appeared to be significant for the curvature of the third mode, this mode is normally not the dominant mode in the building seismic responses. Therefore, the difference may not significantly affect the response calculation accuracy.

The MPA results were further used to determine the story shear and overturning moment of each individual mode. The story shear contributed by the flexural action $V_{i,wall}(x,\ t)$ was computed by adding up shear forces in all RC walls in that story, whereas the story shear contributed by the shear action $V_{i,frame}(x,\ t)$ was computed by adding up shear forces in all columns and masonry infill walls, as depicted in Figures 5 and 6 by the blue and red lines, respectively. Their sum is equal to the story shear $V_i(x,\ t)$, represented by the black line. Similarly, the overturning moment contributed by the flexural action $OM_{i,wall}(x,\ t)$ was determined by summing up the moments of the geometric center of the tower's floor plan based on the internal forces (axial force and bending moment) of all RC walls. The overturning moment contributed by the shear action $OM_{i,frame}(x,\ t)$ was determined by summing up the moments of the center based on the internal forces (axial force and bending moment) of all columns and masonry infill walls. The moments $OM_{i,wall}(x,\ t)$ and $OM_{i,frame}(x,\ t)$ are plotted in Figures 5 and 6 and indicated by the blue and red lines, respectively. The sum of these moments is the story overturning moment $OM_i(x,\ t)$, represented by the black line.

The comparisons in Figures 5 and 6 indicate that CSFCBM can provide reasonably accurate estimates of story shear and overturning moment from the base to the top of the case study buildings in all three transverse modes. Moreover, the load sharing between the RC walls and frames can be determined with reasonable accuracy for all these modes. A comparison of buildings S1 and B1 indicates that the load sharing proportions were different, which can be explained by parameter α. For instance, the lateral load resistance mechanism of building B1 with α as low as 1.43 was expected to be more dominated by the flexural action; hence, the shear in RC walls was generally substantially greater than that in frames. Building S1, with a higher value of α (α = 2.88), was expected to have an increased shear action, and this increase in the proportion of shear in frames was shown by FEM results and was well predicted by CSFCBM.

Noted that the comparisons were made not only for S1 and B1 in the x direction but also for four case study buildings in both the x and y directions. Similar accuracies were obtained in all cases. However, due to space limitations, only two cases are presented in this paper. More details on the verification of the CSFCBM can be found in Suwansaya [37]. In the past, CSFCBM has been typically used for estimating story-level responses, such as story shear and inter-story drift [11,16–19]. In this study, we demonstrate that it can be used for estimating the internal load sharing between frames and shear walls as well.

4.3. Estimation of α-Value

In Section 4.2, parameter α was determined using period ratio T_1/T_2, which was obtained from an eigen analysis of the FEM of the building. If the FEM was not available, the first-mode period T_1 could be estimated using empirical formulas (Section 3). However, the second-mode period T_2 cannot be estimated reliably. In such a case, parameter α may need to be determined using another method.

One possible method is to calculate a structural index and use it to estimate the value of α. This index should exhibit a strong relationship with α and must measure the ratio of the shear action to flexural action of the building. At the same time, the building information required for calculating this index should be as minimal as possible, and the calculation involved should be simple for practical applications. One index that fits these requirements is GA_o/EI_o, where GA_o and EI_o are indexes that measure the shear and flexural rigidities of the building, respectively. EI_o can be defined as the sum of the flexural rigidity of all RC walls of a typical story in a building.

$$EI_o = \sum_{j=1}^{N_w} EI_{wall}(x)_j \tag{23}$$

where $EI_{wall}(x)_j$ denotes the flexural rigidity of the j^{th} RC wall, and N_w indicates the total number of RC walls in a typical story. With a building floor plan showing RC walls and their cross-sectional dimensions, EI_o can be determined easily.

In the case of buildings with well-isolated RC walls (no coupled walls) and the flexural action being predominantly contributed by these RC walls, EI_o is equal to EI of the flexural beam in CSFCBM. However, EI_o is typically not equal to EI owing to the presence of the wall coupling effect and contributions of other building components to the flexural action of the building. Despite this, EI_o is expected to exhibit a strong relationship with EI. GA_o can be calculated as follows:

$$GA_o = \frac{12\sum_{j=1}^{N_c} EI_{col}(x)_j}{h^2} \tag{24}$$

where $EI_{col}(x)_j$ denotes the flexural rigidity of the j^{th} column at the typical story, N_c indicates the total number of columns, and h represents the typical story height. With a building floor plan showing all columns and their cross-sectional dimensions, GA_o can be easily determined.

If all beams (or slabs) in the frame system are extremely stiff compared with the columns, each story deforms in the shear mode, wherein columns are laterally deformed in a double-curvature bending shape. In such cases, the lateral story stiffness of the frame system is equal to GA_o/h. This condition is unlikely to occur in reality. Moreover, there may be a significant contribution of masonry infill walls to the shear action of the building; however, this contribution is not accounted by the index GA_o. Therefore, GA_o is generally not equal to GA of the shear beam in CSFCBM. Nevertheless, GA_o is expected to exhibit a strong relationship with GA.

Table 4 summarizes the structural indexes EI_o and GA_o in the x and y directions obtained using the as-built drawings of the four case study buildings. Additionally, the α value of each building in each direction (x, y) is indicated. In all cases, the typical floor plan properties for the floors just above the podium level were used for this calculation. The relationship between α and the structural index GA_o/EI_o can be determined using these data.

Table 4. Structural indexes and α of the four case study buildings.

Building Name	X Direction				Y Direction			
	S1	**B1**	**B2**	**B3**	**S1**	**B1**	**B2**	**B3**
Height of the building, H (m)	105.0	116.9	59.5	152.5	105.0	116.9	59.5	152.5
First mode period, T_1 (s)	4.420	3.112	1.704	2.717	3.371	5.487	2.701	2.854
Second mode period, T_2 (s)	1.088	0.613	0.410	0.574	0.744	1.457	0.800	0.564
T_1/T_2	4.063	5.077	4.156	4.733	4.531	3.766	3.376	5.060
α	2.88	1.43	2.68	1.80	2.06	3.76	6.58	1.45
EI_o ($\times 10^{12}$ N·m^2)	1.32	9.96	1.35	25.2	3.75	0.88	0.34	20.6
GA_o ($\times 10^{10}$ N)	7.05	2.38	1.28	8.67	10.2	9.56	6.92	8.67
$\sqrt{GA_o/EI_o}$ (1/m)	0.232	0.049	0.098	0.059	0.164	0.329	0.453	0.065

As depicted in Figure 7, α increases linearly in proportion to the increase in $\sqrt{GA_o/EI_o}$. Their relationship can be approximated by the best-fitted linear regression formula (dashed line in Figure 7), as follows:

$$\alpha = 10.9\sqrt{GA_o/EI_o} + 0.85 \tag{25}$$

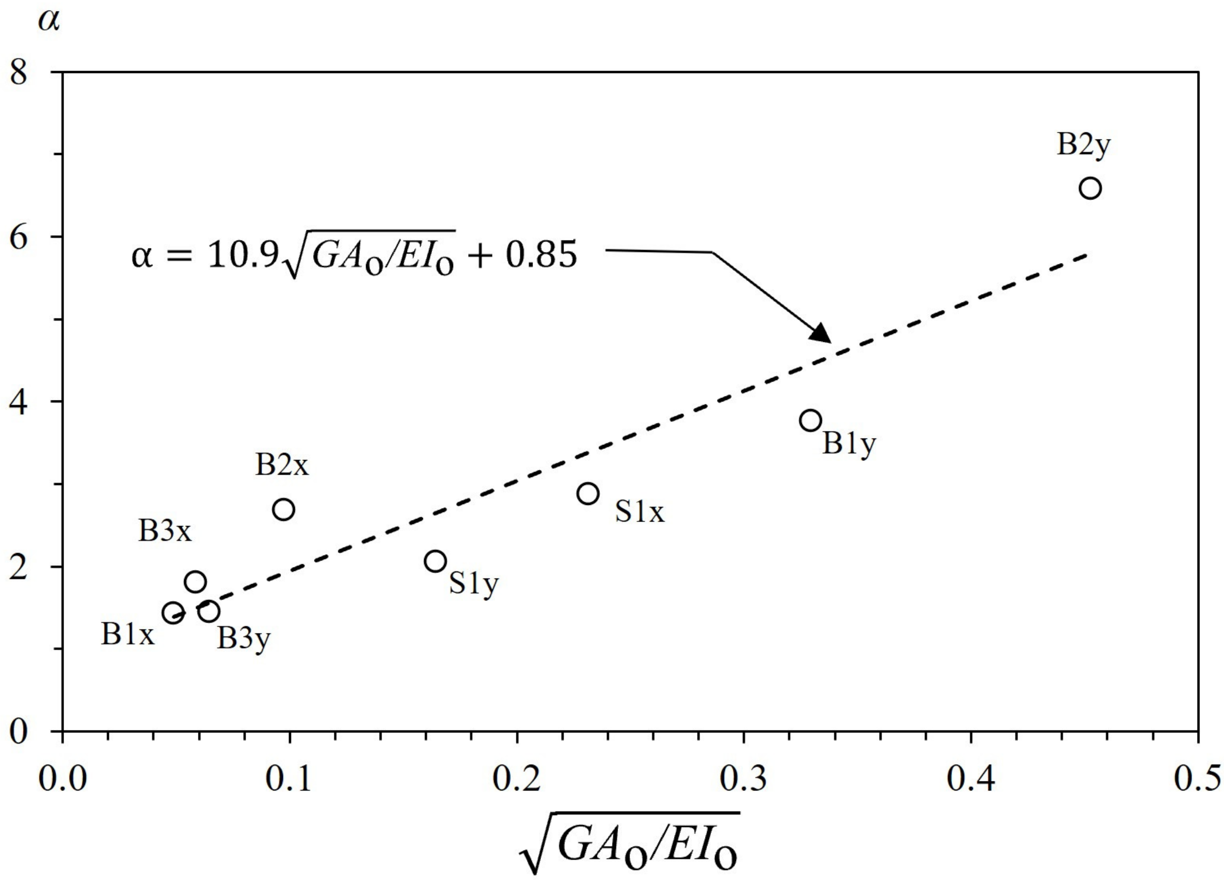

Figure 7. Relationship between α and $\sqrt{GA_o/EI_o}$.

The correlation coefficient (r) of this regression formula was as high as 0.93, indicating a strong correlation between α and $\sqrt{GA_o/EI_o}$. Although only four case study buildings are considered, their results clearly suggest that the α value of other high-rise buildings can be approximately estimated from $\sqrt{GA_o/EI_o}$ using Equation (25). However, the number of samples (eight cases from four buildings) was not sufficient to draw a firm conclusion. Therefore, further investigation with more buildings is necessary to confirm the reliability and accuracy of this approach. This proposed equation is merely an alternative way to estimate the α-parameter based on the properties of the building. There might be a better structural index that exhibits a stronger relationship with the α-parameter.

5. Modal Hysteretic Model

5.1. Modal Hysteretic Behavior

The modal hysteretic behavior of a high-rise building is the result of the combined responses of various structural and non-structural components within the building. This modal hysteretic behavior is different in each vibration amplitude, and monotonic and cyclic MPAs can be used to analyze it. The monotonic MPA enables us to observe the sequence of damage to various components of the structure when the vibration amplitude or lateral displacement increases. Typically, monotonic MPA results will be presented in the form of a capacity curve, which defines an envelope of the modal hysteretic response by approximating the lateral strength and deformation capacity of the building. On the other hand, the cyclic MPA directly demonstrates the modal hysteretic behavior of the building at various vibration amplitudes or lateral displacements, varying from a low level to a state close to collapse.

Recently, several monotonic and cyclic MPAs of RC high-rise buildings with various configurations have been carried out [12–14,38]. Their results indicate that the capacity curves of the fundamental mode and other higher modes can be approximately idealized as a trilinear curve, as depicted in Figure 8. In this figure, the capacity curve shows the relationship between the modal base shear ($V_i(0)$) and modal roof displacement ($u_i(H)$). The roof displacements of the i^{th} vibration mode ($u_i(H)$) at points A, B, and C are denoted by $u_{i,c}(H)$, $u_{i,y}(H)$, and $u_{i,u}(H)$, respectively, and the corresponding base shears ($V_i(0)$) are indicated by $V_{i,c}(0)$, $V_{i,y}(0)$, and $V_{i,u}(0)$, respectively.

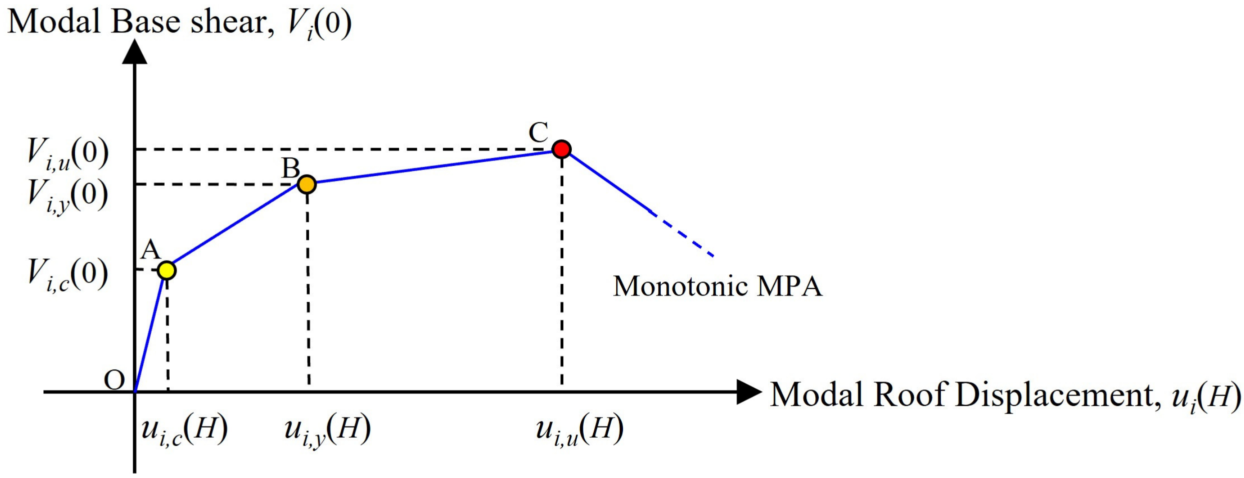

Figure 8. Generalized capacity curve.

In the initial state (between points O and A), the building response is essentially linear elastic with high stiffness, referred to as the initial stiffness. In this state, although certain masonry infill walls may begin to crack, their effect on the capacity curve appears to be insignificant. When the response exceeds point A, a significant reduction is observed in the stiffness, resulting in a softening behavior. The softening effect is found to be caused by flexural cracking in the RC walls at point A. The cracking is typically first formed in the primary RC wall, which has the highest flexural rigidity (EI) and largest cross-sectional dimensions, and is followed by other RC walls. In many cases where RC walls in the buildings are similar in cross-sectional dimensions, their cracking begins at nearly the same level of the roof displacement. As the roof displacement increases from point A to point B, more severe cracking in masonry walls will develop, and some are even crushed, while some RC columns may begin to crack, but all these damages appear to have no significant effect on the softening behavior of the building. The stiffness between points A and B is referred to as the post-crack stiffness.

When the roof displacement exceeds point B, another significant reduction in stiffness occurs owing to the flexural yielding in RC walls. Similar to the cracking at point A, yielding first occurs in the primary RC wall at point B and subsequently occurs in other RC walls. As the roof displacement increases from point B to point C, some RC columns may yield; however, they generally have no significant effect on the post-yield behavior of the building. The stiffness between points B and C is referred to as the post-yield stiffness, which is typically found to be about 0.1 to 0.2 times the post-crack stiffness [12–14,38].

When the response reaches and exceeds point C, there will be a significant lateral strength degradation, and the structure will be about to collapse. It means that some primary lateral load resisting members have already failed (e.g., shear demand has already reached the shear capacity of the primary wall). The calculation beyond this point even by using a nonlinear FEM is not reliable nor accurate. The modal roof displacement at point C, $u_{i,u}(H)$, is approximately two to three times that of point B, $u_{i,y}(H)$. Previous studies [12–14,38] have determined that the modal hysteretic response rarely reaches this drift level, $u_{i,u}(H)$.

Similar to the capacity curve, the cyclic modal hysteretic response behavior can be classified into three different states, namely, linear elastic, flag-shaped, and modified flag-shaped. When the maximum roof displacement is less than $u_{i,c}(H)$ (point A), the cyclic behavior is essentially linear elastic (Figure 9a). When the maximum roof displacement is between $u_{i,c}(H)$ (point A) and $u_{i,y}(H)$ (point B), the cyclic behavior is flag-shaped, as depicted in Figure 9b. When the maximum roof displacement is between $u_{i,y}(H)$ (point B) and $u_{i,u}(H)$ (point C), the cyclic behavior is a modified flag-shaped type, as shown in Figure 9c.

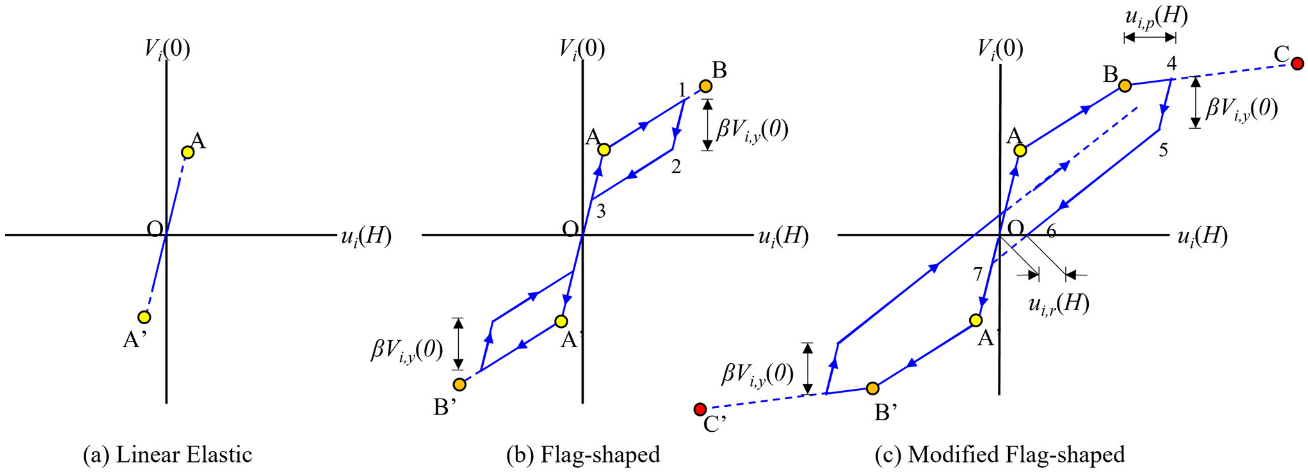

Figure 9. Generalized full cyclic responses.

For the flag-shaped type (Figure 9b), in the loading phase (O→A→1), the response follows the initial stiffness until it reaches point A, where flexural cracking of the primary RC wall starts to form, resulting in a significant stiffness reduction. Subsequently, it follows the post-crack stiffness until it reaches point 1. In the unloading phase (1→2→3→O), the unloading path can be divided into three segments. The first segment is the unloading path from point 1 to point 2 with an unloading stiffness approximately equal to the initial stiffness. The decrease in the base shear is equal to β times $V_{i,y}(0)$. The second segment is the unloading path from point 2 to point 3, where the opening flexural cracks in the RC walls are completely closed. The closing of the crack is primarily caused by the reduction in the bending moment and the effect of the gravity load (axial compression) in these RC walls. The stiffness of this unloading path is approximately equal to the post-crack stiffness in the loading phase. The third segment is the unloading path from point 3 to point O. As all flexural cracks are already closed, the RC walls behave as uncracked walls, exhibiting uncracked (initial) stiffness with no residual deformation when the load reduces to zero.

Based on the aforementioned loading–unloading mechanism, the cyclic modal hysteretic behavior is flag-shaped, which is a nonlinear and self-centering behavior. The width (hoist) of the flag is defined by the β parameter, whose value varies from building to building. A building with a low β value has a narrow flag shape and low hysteretic energy loss, whereas a building with a high β value has a wide flag shape and high hysteretic energy loss. The β value is essentially associated with the crack-closing mechanism. We observed that buildings with high axial compression load (P) in RC walls, caused by the gravity load, tend to have their flexural cracks closed more easily, resulting in low β values. Conversely, in buildings with RC walls having a high number of vertical reinforcement bars, which act as resisting elements of crack closing, flexural cracks tend to be harder to close, resulting in high β values. Therefore, the β parameter is considered to be strongly associated with a dimensionless structural index P/P_s, where P_s denotes the cross-sectional area of the vertical reinforcement rebar (A_s) multiplied by its yield strength (f_y). For buildings with multiple walls, this index should be determined using the parameters of the primary RC wall at its cross-section where flexural cracks occur. More discussion on the β parameter is given in Section 5.2.

When the maximum roof displacement is between $u_{i,y}(H)$ (point B) and $u_{i,u}(H)$ (point C), the cyclic behavior is a modified flag-shaped type, as shown in Figure 9c. In the loading phase (O→A→B→4), the response follows the initial stiffness until it reaches point A, followed by the post-crack stiffness until it reaches point B, where flexural yielding of the RC wall occurs. Subsequently, it follows the post-yield stiffness until it reaches point 4, where a plastic deformation of $u_{i,p}(H)$ is developed. In the unloading phase (4→5→6), the unloading path can be divided into two segments. The first segment is the unloading path from point 4 to point 5, which exhibits an unloading stiffness that is approximately equal to the initial stiffness. The decrease in the base shear is approximately equal to β times $V_{i,y}(0)$. The second segment is the unloading path from point 5 to point 6, which is the zero-load point. At this point, certain flexural cracks in the RC walls remain open owing to the residual plastic strain in the vertical rebars, resulting in a residual lateral deformation $u_{i,r}(H)$. After the loading direction is reversed and loading is increased, these flexural cracks close, and the response rejoins the loading path with the initial stiffness in the opposition direction (point 7).

This modified flag-shaped behavior with residual deformation exhibits a greater hysteretic energy loss compared with the previous state (flag-shaped). Pandey [39] investigated the first-mode residual deformation of three high-rise buildings and determined that this residual deformation relies on the post-yield deformation, and their empirical relationship can be obtained as

$$u_{i,r}(H) = 0.5(u_{i,p}(H))^{1.35} \tag{26}$$

The correlation coefficient (r) of this regression formula is as high as 0.82, indicating a strong correlation between $u_{i,p}(H)$ and $u_{i,r}(H)$. Although this empirical relationship was developed from the first-mode responses, this study assumes that it is applicable to other higher modes as well. Further investigations are required to verify this assumption. However, in most seismic response calculation cases, the modal hysteretic response of higher modes rarely reaches this modified flag-shaped state.

This explanation of hysteretic responses can be used when the structure deforms from the maximum positive to the maximum negative, referred to as the full cycle. However, the structure might not deform in the full cycle when subjected to random earthquake loading. Therefore, a set of hysteretic rules is required to predict the modal hysteretic behavior under several different response paths. Based on the cyclic MPA of three high-rise buildings with different loading histories, Pandey [39] identified a set of hysteretic rules, which can be briefly explained as follows.

Figure 10a depicts the first and second full cycles of the modal hysteretic response. In the first cycle (solid gray line), the loading curve always follows the capacity curve (O→A→B→C) in both directions, and the unloading paths follow the full cycle responses, as depicted in Figure 9. When the loading begins in the second cycle (O→1), denoted by the blue line, the response curve aims toward the previous maximum point (point 1). After it reaches this point, the curve follows the capacity curve until it is unloaded. When it is unloaded (3→4→5), the curve follows the unloading rule for the first cycle until it reaches the residual deformation point (point 5). Subsequently, it is reloaded to the previous maximum point in the opposite direction (point 2), and it follows the backbone capacity curve in the opposite direction. The response curve follows a similar rule when unloaded.

Figure 10b shows the path when the structure is reloaded before it deforms in the opposite direction. When the structure is reloaded from a certain point (point a, b, or c) in the positive direction, the reloading curve aims toward the previous maximum point in that direction (point 2). Conversely, if it is on the negative side, the reloading curve aims toward the previous maximum negative point (point 6). Figure 10c shows the path when the structure is unloaded before reaching the previous maximum point. The unloading curve follows the unloading rule of the full cycle.

The aforementioned hysteretic behaviors are referred to as modal hysteretic rules. A more complete set of modal hysteretic rules was reported by Pandey [39]. For any given vibration mode, if the coordinates of points A and B of its capacity curve and β value are known, then one can construct the modal hysteretic model by following these modal hysteretic rules.

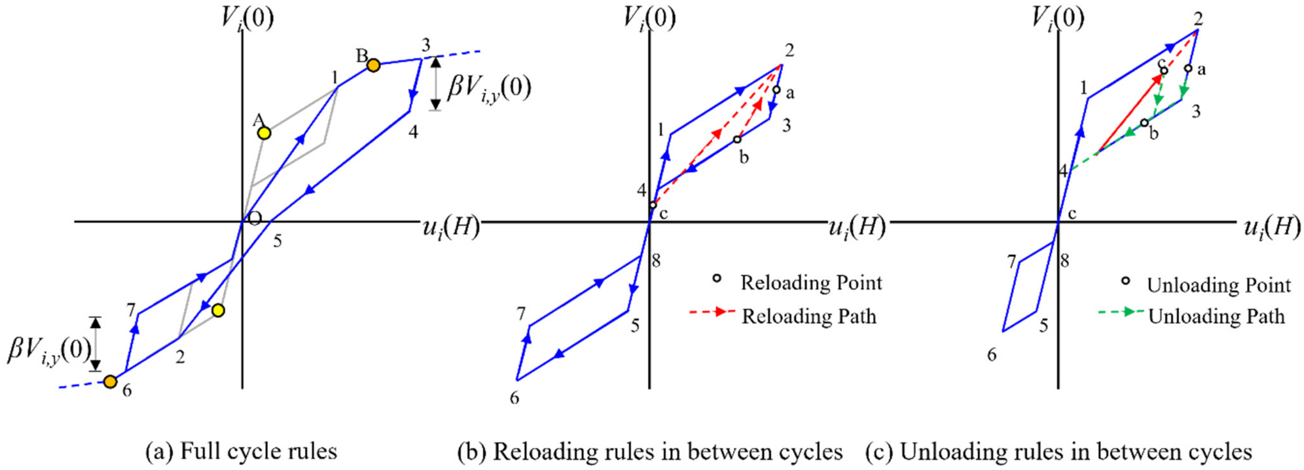

Figure 10. Hysteretic rules [39].

5.2. Construction of the Modal Hysteretic Model Using CSFCBM

As mentioned earlier, monotonic and cyclic MPAs are the direct methods of estimating the coordinates (points A and B) and β value, respectively. However, these are time-consuming and laborious tasks as a nonlinear FEM of the building is required for performing such analyses. Hence, this section explains the method of estimating the coordinates and β value for each vibration mode of the building without using MPAs. The coordinates were determined using CSFCBM, whereas the β value was estimated using the structural index (P/P_s).

As explained in Section 5.1, the primary RC wall begins to crack at point A. Therefore, at this point, the strain at the extreme fiber of the primary wall should reach the concrete cracking limit (ε_{cr}). When the building vibrates in the i^{th} mode, the maximum strain at the extreme fiber of the primary wall at height x above the ground ($\varepsilon_{i,ext}(x,\ t)$) is the sum of the initial compressive strain induced by the gravity load ($\varepsilon_g(x)$) and the flexural strain induced by the lateral deformation of the i^{th} mode ($\varepsilon_{i,f}(x,\ t)$). When $\varepsilon_{i,ext}(x,\ t)$ reaches ε_{cr} at any height x, flexural cracking is expected to form at that height.

$$\varepsilon_{i,ext}(x,t) = \varepsilon_g(x) + \varepsilon_{i,f}(x,t) = \varepsilon_{cr} \tag{27}$$

The cracking limit ε_{cr} can be estimated by dividing the tensile strength (f_t) of the concrete by its elastic modulus (E_c). As recommended by ACI-318 [33], f_t is approximately 0.1 times the expected compressive strength (1.3 $f_c\prime$). As E_c is the modulus at the low-stress level, it is assumed to be approximately 1.5 times the ACI's concrete secant modulus ($4700\sqrt{f_c\prime}$) to account for the nonlinear stress–strain relationship of concrete. Based on these assumptions and approximations, ε_{cr} for concrete with $f_c\prime$ of approximately 35–50 MPa is approximately 100 μmm/mm.

The initial compressive strain at height x ($\varepsilon_g(x)$) depends on the axial compression load in the primary wall ($P(x)$), which is equal to the sum of gravity loads of all floors above that height. On each floor, the gravity load can be estimated by multiplying the distributed gravity load per unit area by the tributary area of the wall. For simplicity, this initial compressive strain is assumed to be uniformly distributed across its cross-section; therefore, it can be estimated as $\varepsilon_g(x) = P(x)/(E_c A_g(x))$, where $A_g(x)$ denotes the gross cross-sectional area of the primary wall at height x. Herein, $A_g(x)$, the tributary area, and the gravity load can be determined using the as-built drawings of the building. In every building, $\varepsilon_g(x)$ increases from zero at the top to the maximum value at the base, as indicated by the solid black line in Figure 11.

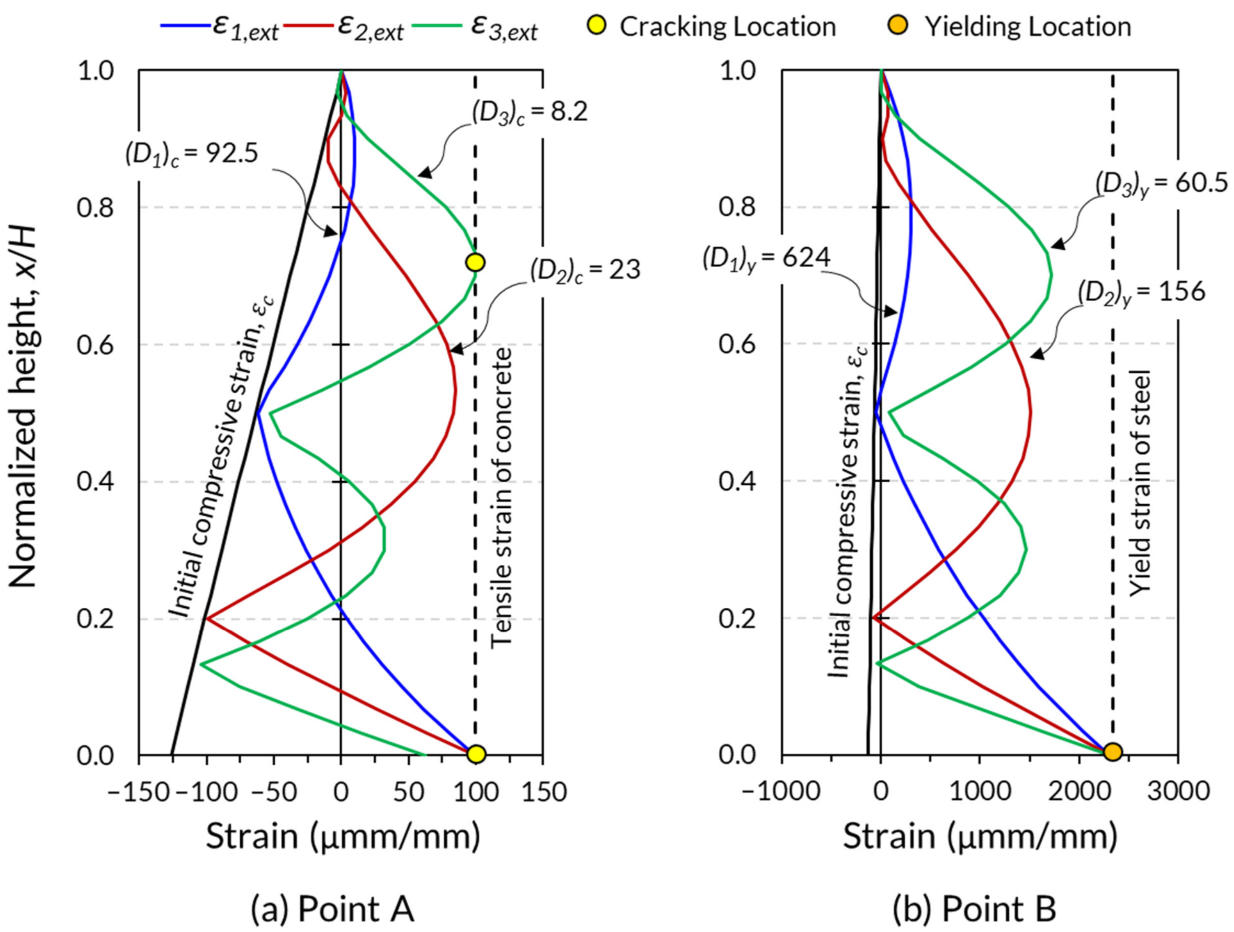

Figure 11. Strain of the primary RC wall of building S1 in the x direction.

The flexural strain at the extreme fiber of the primary wall ($\varepsilon_{i,f}(x,\ t)$) is equal to the absolute curvature ($|\varphi_i(x,\ t)|$) multiplied by the distance from the neutral axis to the extreme tension face (L_t): $\varepsilon_{i,f}(x,\ t) = |\varphi_i(x,\ t)|L_t$. The distance L_t can be determined by a section analysis of the uncracked section of the primary wall. According to the derived relationship of the CSFCBM (Equation (21)), the curvature is linearly proportional to the modal coordinate ($D_i(t)$). The modal coordinate at which flexural cracking occurs in the primary wall (denoted by $D_{i,c}$) can be determined using Equation (27). For instance, when the building deforms in its first mode, cracking occurs at the base when $D_{1,c}$ = 92.5 mm. Alternatively, if the building deforms in its third mode, cracking occurs at $x = 0.7H$ when $D_{3,c}$ = 8.2 mm. Based on Equation (4), the corresponding modal roof displacement at this cracking condition (point A) can be determined as $u_{i,c}(H) = \Gamma_i \phi_i(H) D_{i,c}$.

The next step involves determining the corresponding modal base shear at point A, $V_{i,c}(0)$. Considering that the responses of the i^{th} mode from the initial state (point O) to the cracking point (point A) remain in the linear elastic range, the corresponding governing equation of motion (Equation (1)) should be that of a linear SDOF system with a natural circular frequency ω_i. Therefore, the modal restoring force at the cracking point $F_{si,c}$ of the i^{th} vibration mode can be evaluated as

$$F_{si,c}/L_i = \omega_i{}^2 D_{i,c} \tag{28}$$

Using the relationship between the modal base shear ($V_i(0)$ and F_{si} in Equation (3)), the corresponding modal base shear at point A ($V_{i,c}(0)$) can be determined as

$$V_{i,c}(0) = \omega_i{}^2 \Gamma_i L_i D_{i,c} \tag{29}$$

Subsequently, the coordinates of point B are determined. As explained in Section 5.1, the flexural yield in the primary RC wall begins at point B. Therefore, at this point, the maximum strain at the extreme fiber of the primary wall should reach the steel yielding limit (denoted by ε_{yl}). For the i^{th} vibration mode, the yielding condition can be expressed as follows:

$$\varepsilon_{i,ext}(x,t) = \varepsilon_g(x) + \varepsilon_{i,f}(x,t) = \varepsilon_{yl} \tag{30}$$

The yielding limit is assumed to be equal to the yield strain of the longitudinal reinforcement steel of the wall, which is computed by dividing its expected yield strength (1.17 f_y) by its elastic modulus (E_s). For typical steel reinforcement bars with f_y = 400 MPa, the yielding limit (ε_{yl}) is 2340 μmm/mm.

As explained earlier, the flexural strain at the extreme fiber of the primary wall ($\varepsilon_{i,f}(x,\ t)$) is equal to $|\varphi_i(x,\ t)|L_t$. However, in this case, the distance L_t has to be determined by a section analysis of the cracked section of the primary wall because the wall has already been cracked. The section analysis will give us not only the distance L_t but also the nonlinear moment–curvature relationship for the wall section under the axial compression load $P(x)$. As flexural yielding may occur at any height above the ground, the section analysis should theoretically be conducted for several different heights. However, since the distance L_t may not vary much along the height, and flexural yielding typically occurs at the base region (see Figure 11b), it is reasonable to first check this yielding condition by using the distance L_t of the base section of the primary wall. If it turns out that yielding may occur at any other height, one can revise the calculation of L_t for the wall section at that height.

Assuming that the vibration mode shapes remain approximately unchanged even after cracking or yielding of RC walls, the relationship between the bending curvature and the modal coordinate (D_i) applies as stipulated by Equation (21). The modal coordinate at which the flexural yielding occurs in the primary wall (denoted by $D_{i,y}$) can be determined using Equation (30), as illustrated graphically in Figure 11b. Finally, based on Equation (4), the corresponding modal roof displacement at this yielding condition (point B) can be determined as $u_{i,y}(H) = \Gamma_i \phi_i(H) D_{i,y}$.

The corresponding modal base shear at point B ($V_{i,y}(0)$) can be approximately estimated using the following four-step procedure. Step 1 is to determine the overturning moment at the base of the primary wall at this point. Step 2 is to estimate the corresponding overturning moment at the base resisted by all the RC walls of the building. Step 3 is to estimate the corresponding overturning moment at the base resisted by all components (walls, frames, etc.) of the building. Step 4, which is the final step, is to determine the corresponding base shear of the building.

In step 1, at point B, the flexural yielding occurs in the primary wall, where the strain at an extreme fiber at a certain height x reaches the yielding limit (ε_{yl}). From the section analysis, the yielding moment occurring at that height can be determined. If yielding occurs at the wall base (x = 0), then this moment is the base overturning moment at the yielding point. However, if yielding occurs at any other height x, then the corresponding base overturning moment can still be estimated since the bending curvature throughout the entire height at this yielding point is known (see also Figure 11b).

In step 2, since all RC walls in the building are laterally deformed in the same shape, all RC walls exhibit the same bending curvature profiles. We can then estimate the corresponding base overturning moment of each individual RC wall at this yielding point. This estimate requires the cross-sectional properties of every RC wall and its section analysis. By assuming that all RC walls are isolated (i.e., no coupled walls), the overturning moment at the base resisted by all RC walls, $OM_{i,wall,y}(0)$, can be estimated by summing the base overturning moments of all individual walls. In reality, there might be coupled walls in the building. However, as long as the effect of coupling is not significant, the "isolated wall" assumption should be approximately valid. Note that this estimate can be further simplified by considering that in most cases, all RC walls yield at the base, and their yielding occurs at the roof displacement close to $u_{i,y}(H)$. In such cases, $OM_{i,wall,y}(0)$ can be approximately estimated by summing all the yielding moments at the wall bases.

In step 3, the overturning moment at the base resisted by all components (walls, frames, etc.) of the building is to be evaluated; this moment is denoted as $OM_{i,y}(0)$. According to CSFCBM, $OM_{i,wall,y}(0)$ is the base overturning moment of the flexural beam ($OM_i{}^f(0,\ t)$), and $OM_{i,y}(0)$ is the combined base overturning of the flexural and shear beams ($OM_i{}^t(0,\ t)$). By using Equations (19) and (20), the ratio of these two moments can be determined. Therefore, $OM_{i,y}(0)$ can be estimated as

$$OM_{i,y}(0) = \frac{OM_i^t(0,t)}{OM_i^f(0,t)} OM_{i,wall,y}(0) \tag{31}$$

Note that CSFCBM was created to approximately represent the building in the linear elastic range. As the yielding point B is well beyond this range, the model's predictions for $OM_i{}^f(0,\ t)$ and $OM_i{}^t(0,\ t)$ are inaccurate. However, by checking with all case study buildings, the ratio of these two moments was found to be accurately predicted by CSFCBM, even up to this yielding point.

In step 4, the modal base shear at point B ($V_{i,y}(0)$) is determined. Throughout this study, the deformation shape of the building in the i^{th} mode was assumed to remain identical to that of the i^{th} elastic mode shape, even after cracking or yielding. By this assumption, the modal inertia force pattern also remains unchanged. Consequently, the base shear and base overturning moment of this mode are both proportional to F_{si}/L_i, as indicated in Equations (3) and (5), respectively. The ratio between them is constant, and as a result, $V_{i,y}(0)$ can be determined from $OM_{i,y}(0)$ by

$$V_{i,y}(0) = \frac{OM_{i,y}(0)}{H_{i,eff}} \tag{32}$$

where $H_{i,eff}$ denotes the effective modal height, determined as follows:

$$H_{i,eff} = \frac{\sum_{j=1}^{N} x_j m_j \phi_i(x_j)}{\Gamma_i M_i} \tag{33}$$

After the coordinates at points A and B in each vibration mode are determined by the procedures explained above, the next (and final) step is to estimate the β value, which is considered to be strongly associated with dimensionless structural index P/P_s of the primary wall. To determine the relationship between β and P/P_s, cyclic MPAs were performed for the first three modes of all four case study buildings. The maximum roof displacements of these MPAs were set between points A and B to obtain the clearest flag-shaped relationship between $V_i(0)$ and $u_i(H)$. Subsequently, a flag-shaped hysteretic model with a certain β value was mapped to the result. The mapping process was repeated iteratively with different coordinates of points A and B and different β values by trial and error until the hysteretic model best fit the result, particularly the area enclosed by the hysteretic loop (flag area).

The best-fitted β values from all study cases are plotted against their corresponding P/P_s in Figure 12. Their relationship can be approximated by the best-fitted linear regression formula (dashed line in Figure 12), as follows:

$$\beta = -0.13(P/P_s) + 0.40 \tag{34}$$

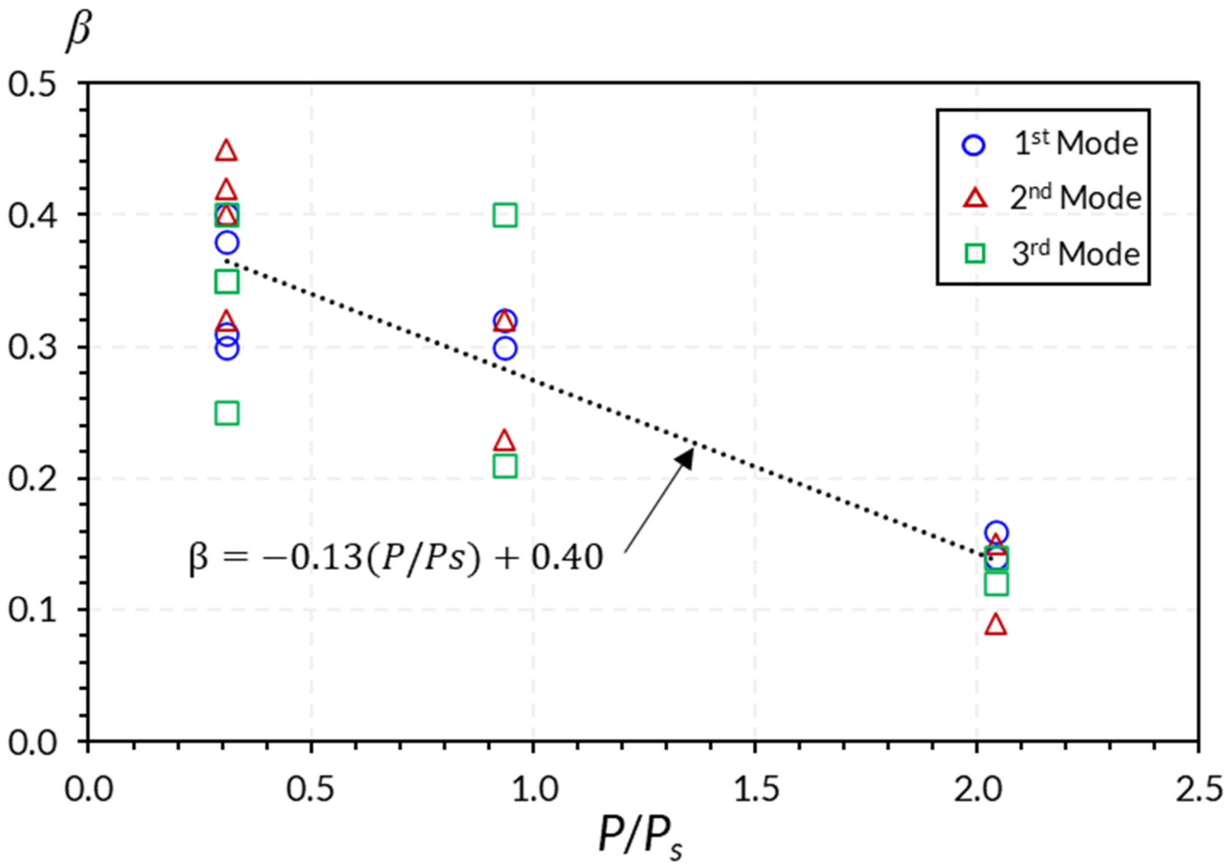

Figure 12. Relationship between β and P/P_s.

The correlation coefficient (r) of this regression formula is as high as 0.75, indicating a strong correlation between β and P/P_s. The result clearly indicates that the β value of other high-rise buildings can be approximately estimated from P/P_s using the above formula. Further investigation on this β–P/P_s relationship using more case study buildings is recommended to confirm the reliability and accuracy of this approach. There might be a better structural index that has a stronger relationship with β.

It should be noted that if a linear FEM of a high-rise building is available, there is no need to construct the building's CSFCBM since the required relations and parameters in this section can be obtained from its linear FEM.

5.3. Verification of the Modal Hysteretic Model

In this sub-section, the accuracy of the proposed procedure for estimating the modal hysteretic model is verified. First, the coordinates at points A and B computed using the procedures explained in Section 5.2 are checked by comparing them with those determined directly from the capacity curves. These curves are obtained from the monotonic MPA for the first three modes in both the x and y axes of all four case study buildings. Comparisons of the normalized modal base shears and roof drift ratios at points A (cracking) and B (yielding) are illustrated in Figure 13. It should be noted that the roof drift ratios can be calculated as the roof displacement divided by its height (H), presented in percentage units, whereas the normalized modal base shears can be calculated as the base shears divided by the building's weight (W). The results indicate that the coordinates at points A and B can be estimated with reasonable accuracy using the proposed procedure.

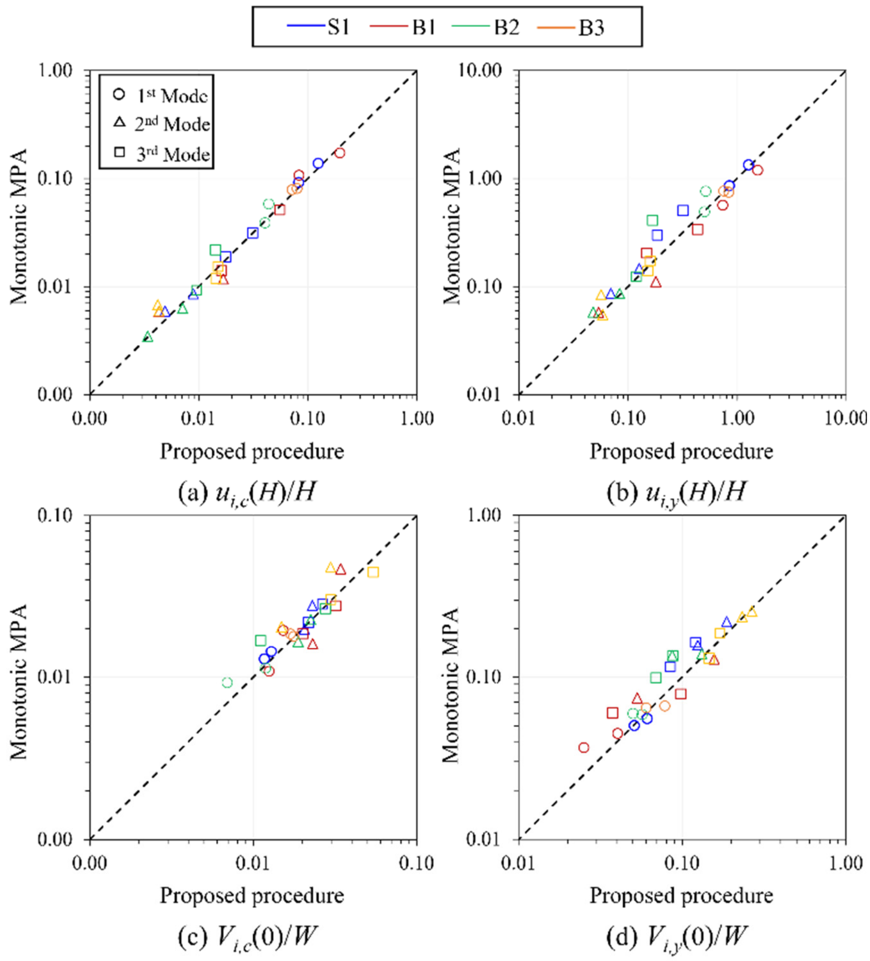

Figure 13. Coordinates at points A and B of the capacity curve.

Second, the modal hysteretic models generated from the coordinates (point A and B) and β values estimated using the proposed procedure are verified by comparing them with those determined directly from the cyclic MPA. In these models, the hysteretic rules and residual deformation relationship developed by Pandey [39] are followed, and the post-yield stiffness is assumed to be 0.2 times its post-crack stiffness for estimating the response beyond point B. The comparison is presented as cycle-by-cycle plots of the modal hysteretic responses of building B2 on the x axis, as depicted in Figure 14. Four levels of displacement amplitude were selected for this comparison, namely, low ($0.1u_{i,y}(H)$), middle ($0.5u_{i,y}(H)$), yield ($1.0u_{i,y}(H)$), and post-yield ($1.5u_{i,y}(H)$). The results verify that the estimated modal hysteretic models concur reasonably well with those obtained from the cyclic MPA in all displacement ranges. Similar verification was also conducted for three other case study buildings in both directions, and similar good results were obtained, confirming the applicability of the proposed procedure. More details on the verification of the developed modal hysteretic model can be found in Suwansaya [37].

It should be noted that this hysteretic model is novel, so it is not available in any conventional software packages. Therefore, we created a personal version subroutine for this hysteretic model using C++ code that can used with the Opensees platform [40]. This subroutine is shown as a Supplement File of this article.

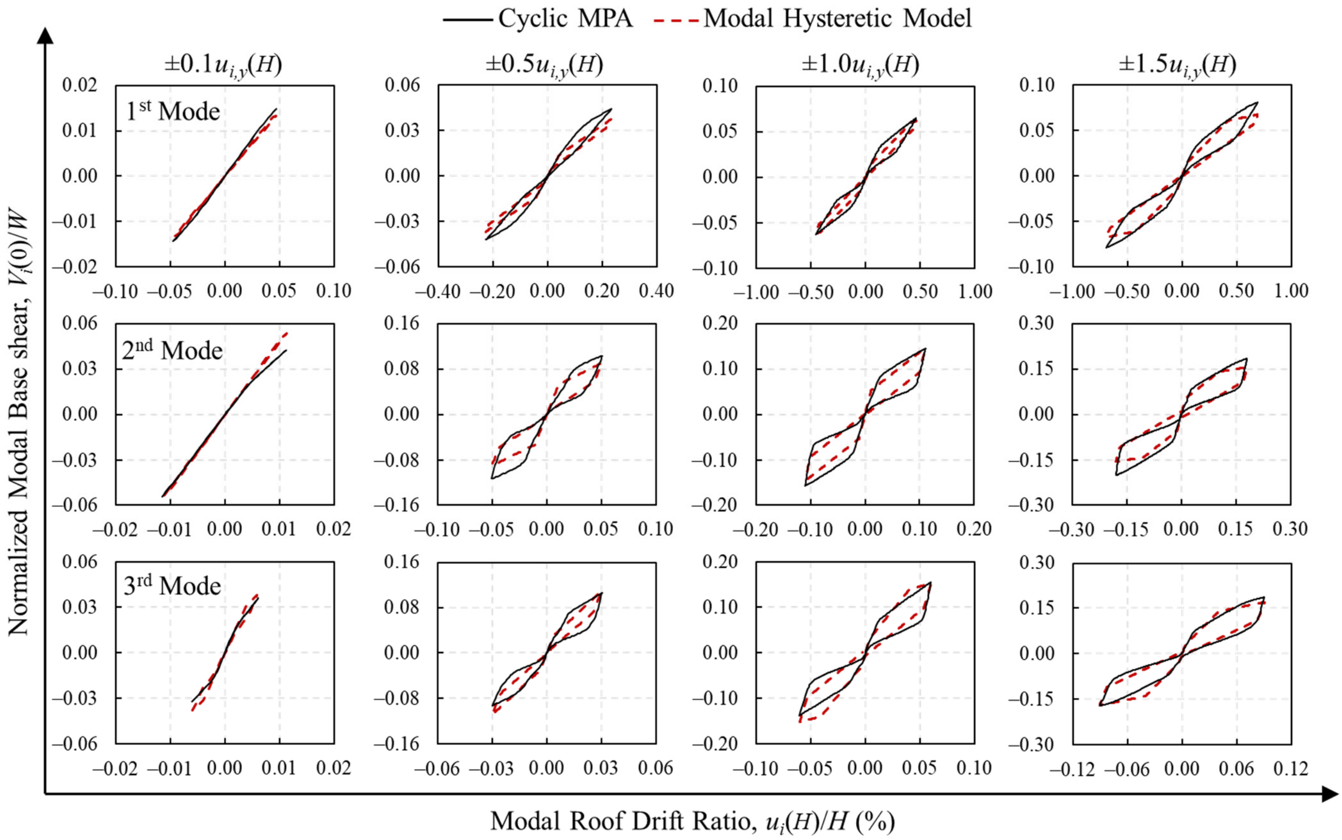

Figure 14. Modal hysteretic responses of building B2 in the first, second, and third modes in the x direction.

6. Verification of the Simplified Procedure

In this section, the validity and accuracy of the proposed simplified procedure based on UMRHA and CSFCBM are carefully checked. Various seismic demands of the four case study buildings under different ground motions were computed using the proposed simplified procedure, and these demands were compared with those computed by NLRHA using 3D nonlinear FEMs. Three pairs of horizontal ground motions, namely, EQ1, EQ2, and EQ3, were selected from the Pacific Earthquake Engineering Research Center (PEER) strong ground motion database for the comparison [41]. These motions were recorded on site class D, with V_{S30} between 180 and 360 m/s, during three different shallow crustal earthquake events with moment magnitudes between 6.8 and 7.3 and source-to-site distances between 2.5 km and 57 km. Figure 15 illustrates the geometric mean response spectrum with a damping ratio of 2.5% for each and every pair. It can be seen that EQ1 exhibits a relatively short-period motion, EQ3 exhibits a relatively long-period motion, and EQ2 is somewhere in between.

To determine the seismic responses of each case study building using the NLRHA procedure, a pair of horizontal motions were applied as simultaneous base excitations along the x and y axes of the building. Its 3D nonlinear FEM is described in Section 4.1. The time histories of story-level responses, such as story shear and interstory drift ratio, and component-level responses, including bending curvature in a wall, were calculated. Additionally, the seismic demands, including the positive and negative maximum responses, were determined. Although this procedure was straightforward, it was highly laborious and time-consuming, as mentioned earlier.

The seismic response analysis performed using the simplified procedure begins with the formation of a CSFCBM for each orthogonal axis (x and y) of the building. The model was formulated using the four basic building parameters, namely, H, m, T_1, and α, obtained from the process described in Section 4.3. With this CSFCBM, important modal properties of the building in the axis of interest can be determined using closed-form formulas, as described in Section 3; these properties include the mode shape (ϕ_i), natural period (T_i), and modal parameters (L_i, M_i, and Γ_i) for i = 1, 2, 3, ... At this step, the governing equation of motion of the i^{th} mode can be formulated in terms of the modal coordinate $D_i(t)$ in a standard format (Equation (1)). The modal damping ratio ξ_i was set to 2.5% in every mode.

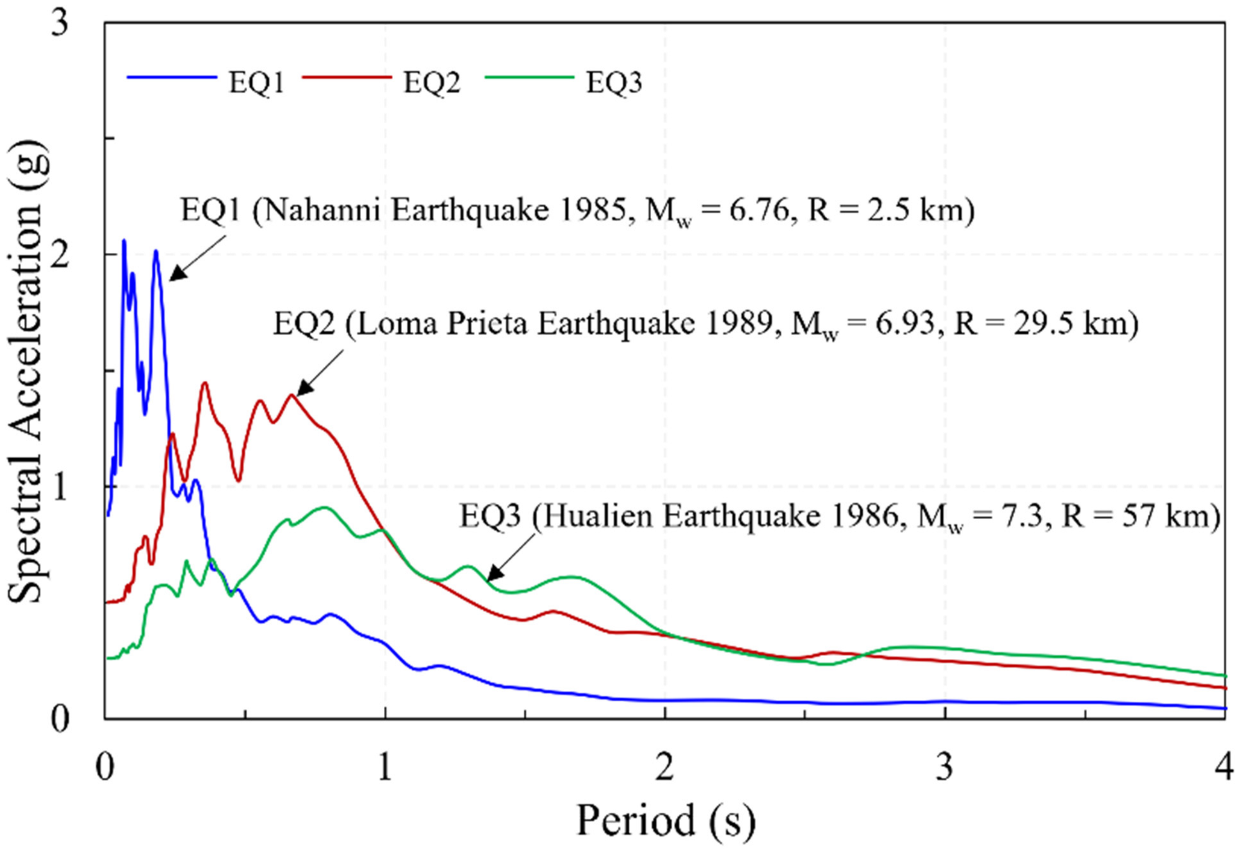

Figure 15. Response spectra of the selected ground motions with 2.5% damping ratio.

Subsequently, the i^{th} modal hysteretic model was formulated using the procedure described in Section 5.2. This model, which is expressed as the relationship between the modal base shear ($V_i(0)$) and modal roof displacement ($u_i(H)$), was then transformed into the corresponding F_{si}–D_i relationship using Equations (2) and (3). Based on this, the modal responses of the building to an input ground motion $\ddot{u}_g(t)$ can be numerically calculated from the standard nonlinear governing equation (Equation (1)), and they are expressed as the time histories of $D_i(t)$ and $F_{si}(t)$. To satisfy the requirement that the sum of the effective participating masses of the building should exceed 90% of the total mass, the responses of the first five transverse modes must be computed for each orthogonal axis. As the modal responses of the fourth and fifth modes are found to be linear elastic in all excitation cases, the calculation can be further simplified for such higher modes by assuming a linear elastic behavior.

At this step, all deformation-related responses, including the lateral floor displacement and interstory drift ratio of the i^{th} mode, were computed from $D_i(t)$, whereas all force-related responses, including the story shear and story overturning moment, were computed from $F_{si}(t)$ using the procedure described in Section 2. By direct summing the responses of all significant modes, which include five modes each on the x and y axes, the time histories of various seismic responses can be obtained, and the corresponding seismic demands can be determined.

Figure 16 shows examples of the computed seismic responses of building B3 to EQ1. Figure 16a depicts the modal base shear of the first five modes in the x axis computed using the simplified procedure. As can be observed, the modal base shear of the second mode is the highest among those of all participating modes. Their sum, the base shear, as shown in Figure 16b, is also dominated by the contribution from the second mode and is well matched with that computed by the NLRHA procedure. The latter is obtained by adding the shear forces of all RC walls, columns, and masonry infill walls at the base of the building. The base shear demand from the NLRHA procedure, as denoted by the white dot, is extremely close to that of the simplified procedure denoted by the red dot. A similar comparison is also made for the story shear at the 13th floor, which is approximately one-fourth of the building height; the results concurred adequately in this case as well.

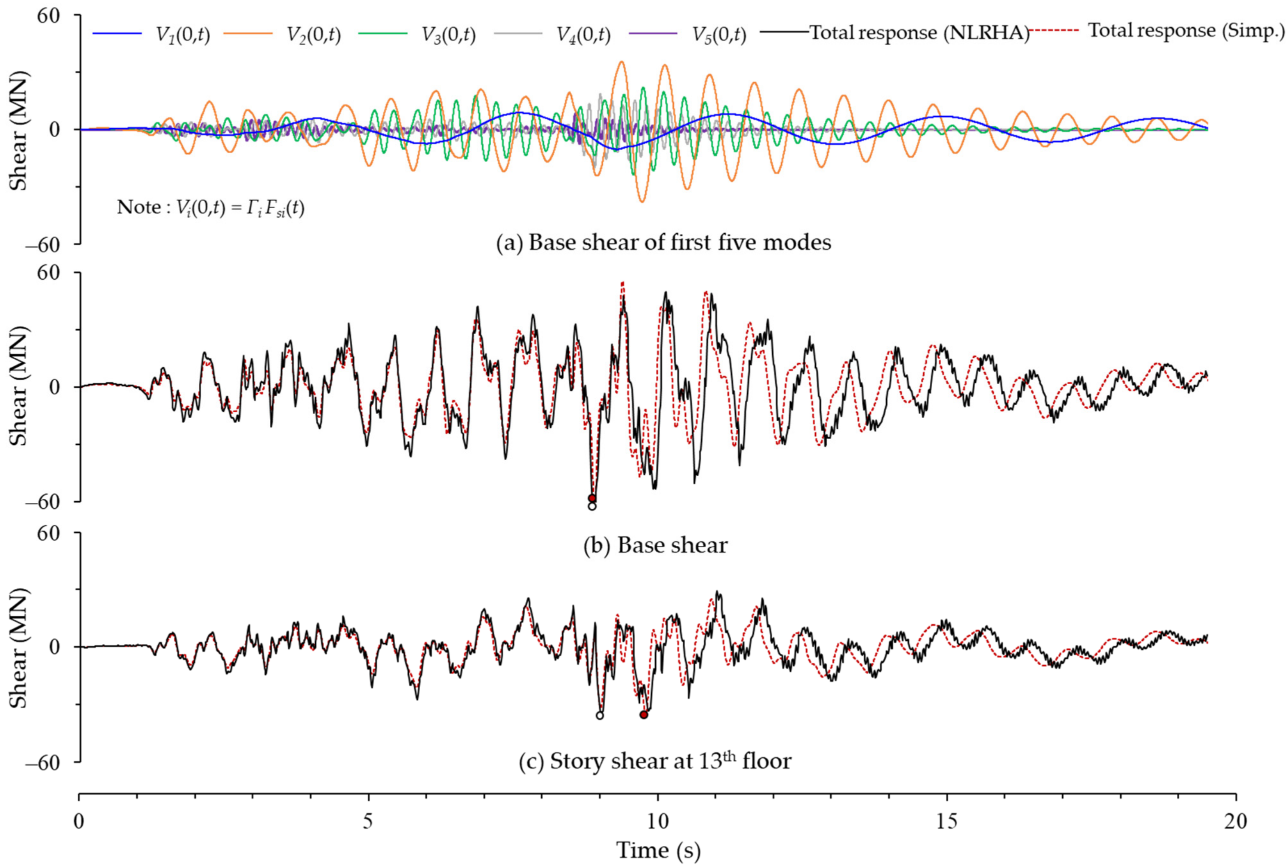

Figure 16. Modal base and story shear time history of building B3 in the x axis caused by EQ1.

Figure 17 illustrates the comparison of various story-level seismic demands of building B3 subjected to EQ1, EQ2, and EQ3 computed using the two procedures. In all cases, reasonably adequate concurrence was obtained, confirming the reliability and accuracy of the simplified procedure. The figure also includes the contributions to seismic demands from each individual mode computed using the simplified procedure. The contributions from all five modes to the story shear demand are found to be significant, and none of them can be neglected. Conversely, the lateral displacement and interstory drift ratio demands are well dominated by the contributions from the first two modes; the contributions from other higher modes can be ignored. These results provide an improved understanding of the contributions from different vibration modes to various seismic demands.

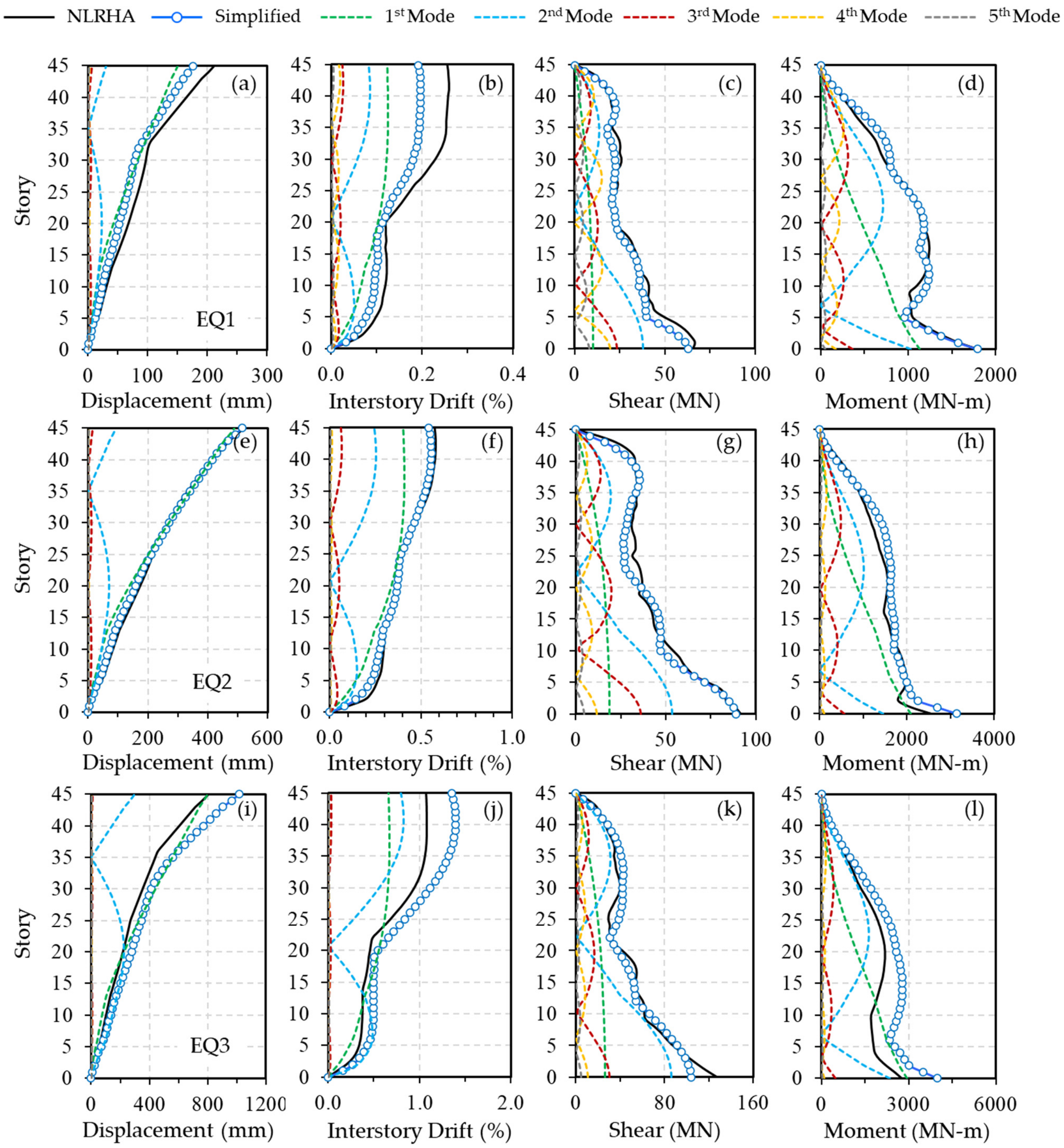

Figure 17. Comparison between various responses of the simplified and NLRHA procedures for all ground motion of building B3 in the x axis (**a**) Floor displacement under EQ1, (**b**) Interstory drift under EQ1, (**c**) Story shear under EQ1, (**d**) Story overturning moment under EQ1, (**e**) Floor displacement under EQ2, (**f**) Interstory drift under EQ2, (**g**) Story shear under EQ2, (**h**) Story overturning moment under EQ2, (**i**) Floor displacement under EQ3, (**j**) Interstory drift under EQ3, (**k**) Story shear under EQ3, (**l**) Story overturning moment under EQ3.

In addition to story-level seismic demands, component-level seismic demands play a significant role in the building's seismic evaluation. Although CSFCBM can be used to estimate the responses contributed by all RC walls and frames, it cannot be used to determine the individual component responses. Therefore, several assumptions were introduced to distribute such responses to individual component responses. Two shear walls of building

B3, a C-shaped shear wall and a box core wall (Figure 18), were selected to demonstrate the estimation of the responses in each individual wall using the simplified procedure.

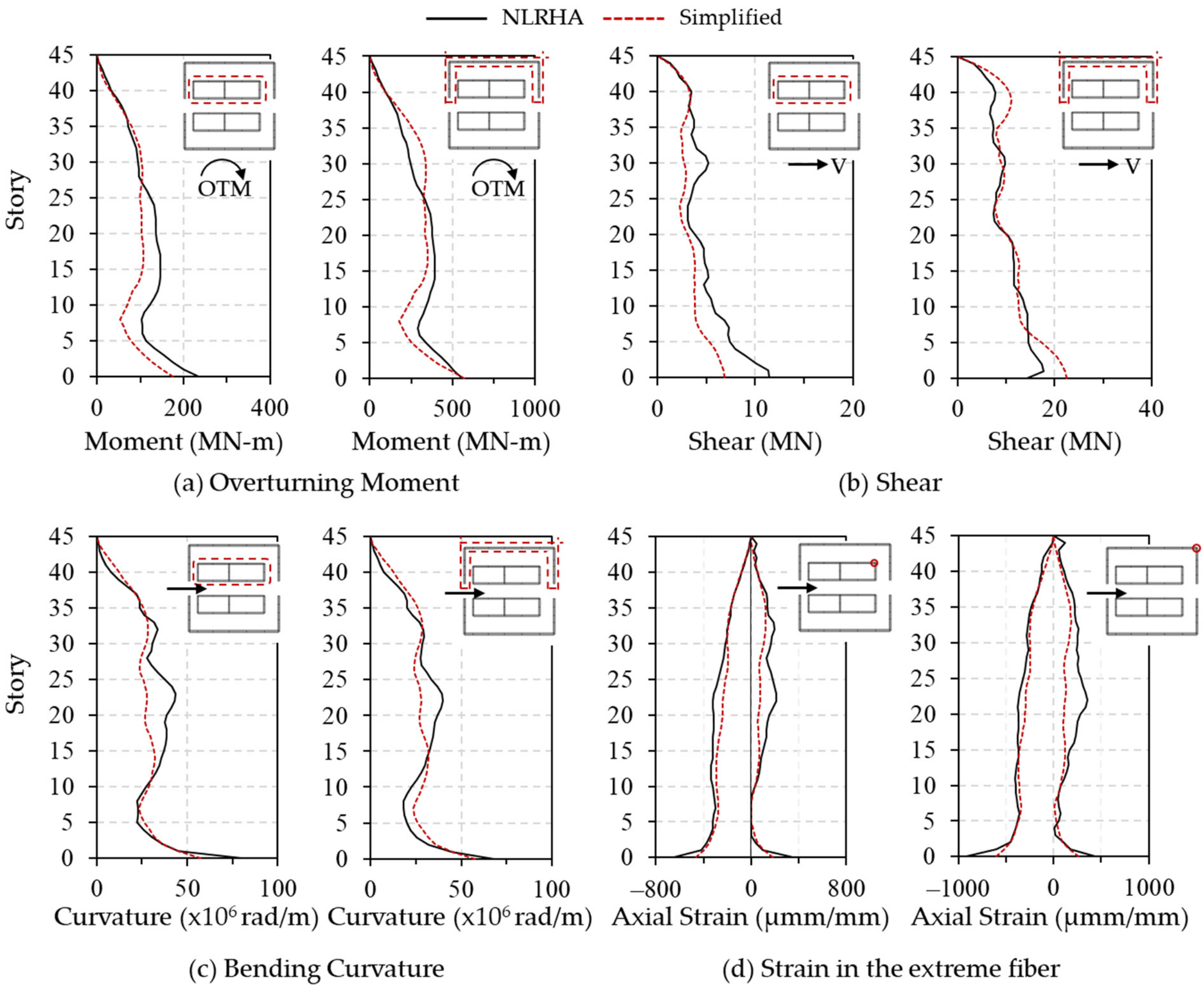

Figure 18. Comparison of the component level responses caused by EQ1 in the x direction for building B3 using the simplified and NLRHA procedures.

Assuming that the vibration mode shapes, and modal inertia loads of the i^{th} mode remain approximately unchanged during the response time history, the force-related responses contributed by all RC walls of the i^{th} mode, such as the story shear and overturning moment, can be determined by multiplying the force-related responses of the i^{th} mode with the modal force contribution of the flexural beam to the total responses (Equations (17)–(20)). For example, the story shear contributed by all RC walls of the i^{th} mode ($V_{i,wall}(x,\ t)$) can be determined by multiplying the story shear of the i^{th} mode ($V_i(x,\ t)$) with the ratio of modal shear force in the flexural beam ($V_i^{\ f}(x, t)$) to the total responses ($V_i^{\ t}(x, t)$) in CSFCBM. To distribute these force-related responses among the RC walls, all RC walls are assumed to be isolated; hence, their bending curvature profiles of the i^{th} mode are identical. Based on this assumption, the story shear and overturning moment of the i^{th} mode in each individual wall ($V_{i,wall}(x,\ t)_j$ and $OM_{i,wall}(x,\ t)_j$) are proportional to the ratio of its flexural rigidity to the total flexural rigidity in that story. The total flexural rigidity can be determined by adding the flexural rigidity of all RC walls in a specific story. Therefore, $V_{i,wall}(x,\ t)_j$ and $OM_{i,wall}(x,\ t)_j$ can be estimated as follows:

$$V_{i,wall}(x,t)_j = \frac{EI_{wall}(x)_j}{\sum_{j=1}^{N_w} EI_{wall}(x)_j} V_{i,wall}(x,t) \tag{35}$$

$$OM_{i,wall}(x,t)_j = \frac{EI_{wall}(x)_j}{\sum_{j=1}^{N_w} EI_{wall}(x)_j} OM_{i,wall}(x,t) \tag{36}$$

The flexural rigidity of each individual wall ($EI_{wall}(x)_j$) can be determined using the gross properties specified in the as-built drawings. Although each individual wall might crack or yield at any level, resulting in changes in its flexural rigidity, we determined that this ratio computed under gross properties accurately distributes the responses among all RC walls in all case study buildings. The force-related responses of each wall of the i^{th} mode can be combined using Equation (6) to determine the force-related demands. Figure 18a,b show examples of the computed story shear and overturning moment demands of the two RC walls in building B3 when subjected to EQ1. The results indicate that the simplified procedure computes responses that are reasonably close to those computed by the NLRHA procedure.

Next, the deformation-related responses, such as the section curvature and strain at the extreme fiber, are determined. The section curvatures of all RC walls of the i^{th} mode can be determined using Equation (21). Similarly, the section curvatures of the i^{th} mode of each wall can be combined using Equation (6) to determine the section curvature demands. On the other hand, the section curvature demands from NLRHA are computed from the maximum of the difference in vertical strains at two opposite extreme fibers of the wall. Figure 18c illustrates examples of the computed section curvature demands of the two RC walls in building B3 when subjected to EQ1. The results indicate that the estimated section curvatures concur well with those obtained from the NLRHA, and the curvatures along the height of both walls are nearly identical. The latter verifies that the "isolated wall" assumption is valid.

Subsequently, the corresponding maximum tensile and compressive strain demands at the extreme fiber of the wall are computed. The strain computed by the NLRHA procedure was determined directly using the strain gauge element attached to the extreme fiber of the wall. The corresponding maximum tensile and compressive strains were determined by the maximum positive and negative strains, respectively. These strains are already included in the initial compressive and flexural strains.

For the simplified procedure, the initial compressive and flexural strains of the i^{th} mode of the wall can be determined using the procedure described in Section 5.2. If the distance from the neutral axis to the tension face (L_t) is used in Equation (22), the flexural-induced tensile strain of the i^{th} mode can be determined. Conversely, if the distance from the neutral axis to the compression face (L_c) substitutes L_t in Equation (22), the flexural-induced compressive strain of the i^{th} mode can be determined. Herein, L_t and L_c were determined from the section analysis of the cracked section at the wall bases. The total flexural-induced compressive and tensile strain can be determined by combining the flexural-induced compressive and tensile strain of the i^{th} mode using Equation (6).

The corresponding maximum tensile and compressive strain demands can be computed by adding the initial compressive strain to the total flexural-induced tensile and compressive strain demands, respectively. Figure 18d depicts examples of the computed maximum tensile and compressive strain demands at the extreme fiber of two RC walls in building B3 when subjected to EQ1. The location of the computed strain is denoted by a circle in this figure; the results match adequately.

Subsequently, the influence of the building configurations, characteristics of ground motion, and intensity level on the accuracy of the simplified procedure are examined. For this purpose, the selected ground motions (EQ1, EQ2, and EQ3) were scaled to eight levels ranging from 0.2 to 1.6 and applied to entire case study buildings using both NLRHA and the proposed procedure. Owing to numerous output seismic demands (96 cases), the maximum normalized base shear ($V_i(0)/W$), normalized base overturning moment ($OM_i(0)/WH$), roof drift ratio ($u_i(H)/H$), and interstory drift ratio (IDR) are primarily considered in this comparison.

Figure 19 depicts a comparison of the seismic demands obtained from the simplified and NLRHA procedures under eight scales of three ground motions. It is noted that the roof drift ratios and interstory drift ratios, which are measured at the top story of the building, are presented in percentage units. The filled and unfilled shapes represent the responses on the x and y axes, respectively. The results indicate that the simplified procedure can accurately estimate the seismic responses of all case study buildings when they are subjected to various intensities and characteristics of ground motion. Even when the buildings are subjected to extremely strong ground motion (scale > 1.0), the simplified procedure estimates the structural responses of the buildings with reasonable accuracy. Furthermore, no discernible effect of building configuration, ground motion characteristics, or seismic intensity is observed on the accuracy of the simplified procedure.

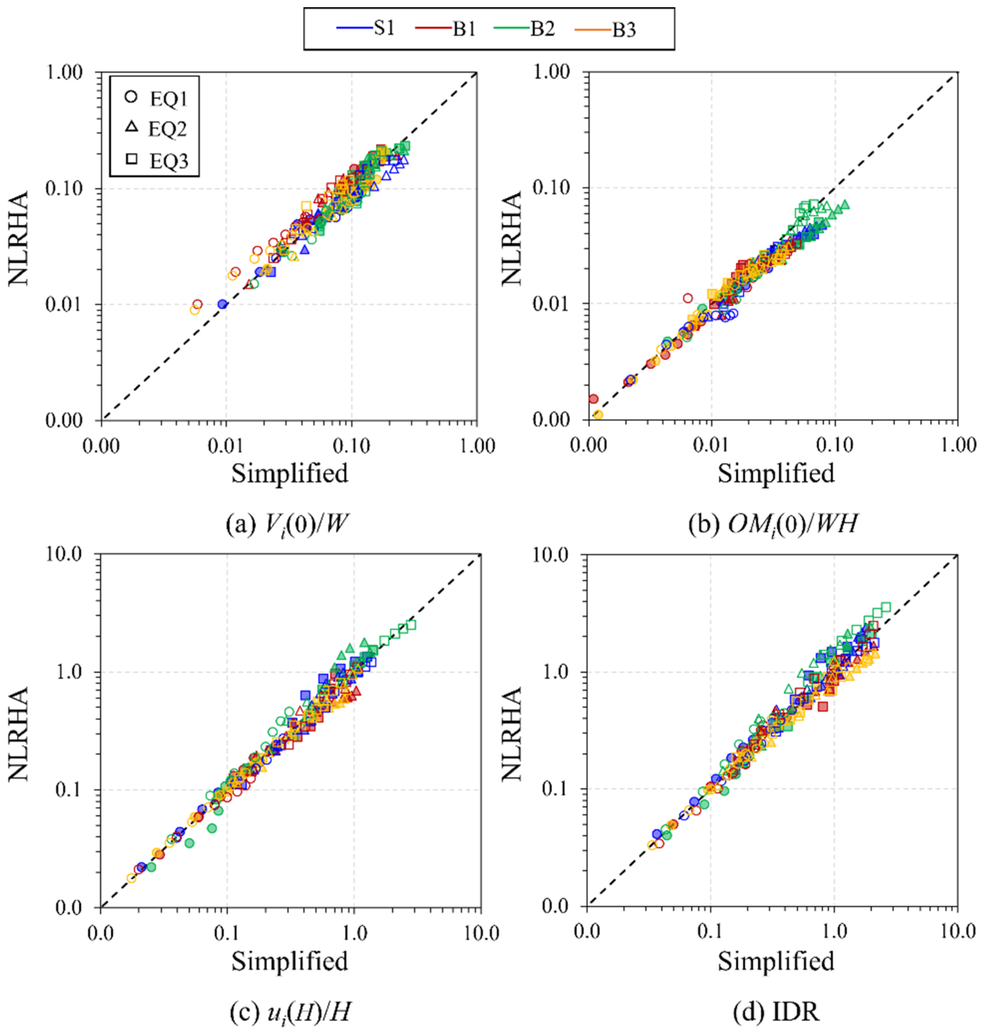

Figure 19. Comparison between various responses of the simplified and NLRHA procedures for all case study buildings excited by the eight levels of EQ1, EQ2, and EQ3.

In this study, an Intel Core i5-11400 32G RAM computer was used for all of the analysis. Table 5 shows the total calculation time for each case study building excited by the eight levels of EQ1, EQ2, and EQ3 using both procedures. The total calculation time is divided into three phases: modeling phase, analysis phase, and post-processing phase. The modeling phase refers to the time to construct the nonlinear FEM for NLRHA procedure and to estimate the six hysteretic models for simplified procedure. The analysis phase refers to the time to perform dynamic analysis of nonlinear FEM for NLRHA procedure and of ten SDOF systems for the simplified procedure for eight levels of EQ1, EQ2, and EQ3 (24 cases). The post-processing phase refers to the time to process the results into the final format for both procedures (Figures 17–19). Obviously, the total calculation time required by the NLRHA procedure varies from about 7 to 45 times that required by the UMRHA procedure. For a large number of analysis cases, NLRHA may require weeks or months to complete the calculations, whereas the simplified procedure can complete them in a few days.

Table 5. Total calculation time of the four case study buildings.

Times (Hour)	S1		B1		B2		B3	
	NLRHA	Simp.	NLRHA	Simp.	NLRHA	Simp.	NLRHA	Simp.
Modeling phase	40.4	1.0	80.5	1.0	30.2	1.0	137.0	1.0
Analysis phase	44.4	1.0	88.7	1.0	33.2	1.0	150.8	1.0
Post-processing phase	13.5	8.3	26.8	7.8	10.1	7.6	45.7	8.3
Total calculation	98.3	10.4	196.0	9.7	73.4	9.6	333.5	10.3

7. Conclusions

This study presents a simplified analysis procedure for estimating the inelastic seismic responses of numerous high-rise buildings with RC shear walls. The proposed procedure was developed from the UMRHA procedure and the CSFCBM. The UMRHA procedure was used to compute the inelastic seismic responses mode by mode, with each vibration mode acting as a nonlinear SDOF system. Because such a model requires knowledge of modal properties and modal hysteretic behavior, the former can be determined by a cyclic MPA of a nonlinear FEM, and the latter can be determined by an eigen analysis of a linearized FEM. However, creating such a model necessitates a significant amount of effort and expertise. Therefore, CSFCBM was introduced to avoid the use of a nonlinear FEM, allowing rapid computation of the inelastic seismic responses of high-rise buildings. Four high-rise buildings with RC shear walls that have different floor plan configurations, shear wall arrangements, and heights ranging from 19 to 45 stories were used to verify its accuracy. The results show that the proposed procedure can estimate the nonlinear seismic demands of these buildings with reasonable accuracy, at both the story and the component level. The proposed procedure has several possible applications due to the advantages of extremely low computational time, minimal data requirements, and minimal use of a nonlinear technique. It can be used to estimate the seismic damage and losses of many high-rise buildings in a city in the event of an earthquake. It can also be used in the preliminary design phase of a high-rise building to quickly assess various seismic design options. However, the proposed procedure has the limitation of being based on several empirical relationships derived from the four case study buildings. Further research including additional buildings is required to confirm the accuracy and reliability, as there might be better relationships that can be used to determine the required parameters (for example, α and β). In such cases, the proposed procedure's accuracy can be improved further.

Supplementary Materials: The following supporting information can be downloaded at: https://www.mdpi.com/article/10.3390/buildings13030670/s1.

Author Contributions: The authors confirm contributions to the article as follows: study conception and design, P.S. and P.W.; data collection, P.S.; analysis and interpretation of results, P.S.; draft manuscript preparation, P.S. and P.W. All authors have read and agreed to the published version of the manuscript.

Funding: This research project was supported by Asian Institute of Technology. The APC was funded by Department of Civil and Infrastructure Engineering.

Data Availability Statement: We are willing to share our data if one requires. Here is the shared folder via google drive. https://drive.google.com/drive/folders/0B_Ez-Tl0wm4gLXNDakI2eXQwWW8?resourcekey=0-_sswg1QwCNwTwOda3_OEyQ&usp=sharing (accessed on 8 December 2022).

Conflicts of Interest: The authors declared no potential conflicts of interest with respect to the research, authorship, and/or publication of this article.

References

1. Maffei, J.; Yuen, N. Seismic performance and design requirements for high-rise buildings. *Struct. Mag.* **2007**, 28–32. Available online: https://www.structuremag.org/wp-content/uploads/2014/09/F-HighRise-Maffei-Apr07-online-version1.pdf (accessed on 8 December 2021).
2. Kayvani, K. Design of high-rise buildings: Past, present and future. In Proceedings of the 23rd Australasian Conference on the Mechanics of Structures and materials (ACMSM23), Byron Bay, Australia, 9–12 December 2014; pp. 15–20.
3. Guidelines Working Group. *TBI: Guidelines for Performance-Based Seismic Design of Tall Buildings*; PEER Report No. 2010/05; University of California: Berkeley, CA, USA, 2010.
4. Su, R.K.L.; Chandler, A.M.; Sheikh, M.N.; Lam, N.T.K. Influence of non-structural components on lateral stiffness of tall buildings. *Struct. Des. Tall Spec. Build.* **2005**, *14*, 143–164. [CrossRef]
5. Kreslin, M.; Fajfar, P. The extended N2 method taking into account higher mode effects in elevation. *Earthq. Eng. Struct. Dyn.* **2011**, *40*, 1571–1589. [CrossRef]
6. Pekelnicky, R.; Engineers, S.D.; Chris Poland, S.E.; Engineers, N.D. ASCE 41-13: Seismic evaluation and retrofit rehabilitation of existing buildings. In Proceedings of the SEAOC-SEANM Convention, Santa Fe, NM, USA, 12–15 September 2012.
7. American Society of Civil Engineers. *Minimum Design Loads and Associated Criteria for Buildings and Other Structures*; American Society of Civil Engineers: Reston, VA, USA, 2017.
8. Remo, J.W.; Pinter, N. Hazus-MH earthquake modeling in the central USA. *Nat. Hazards* **2012**, *63*, 1055–1081. [CrossRef]
9. Chopra, A.K.; Goel, R.K. *A Modal Pushover Analysis Procedure to Estimate Seismic Demands for Buildings: Theory and Preliminary Evaluation*; Pacific Earthquake Engineering Research (PEER) Centre: Berkeley, CA, USA, 2001.
10. Chopra, A.K.; Goel, R.K. A modal pushover analysis procedure for estimating seismic demands for buildings. *Earthq. Eng. Struct. Dyn.* **2002**, *31*, 561–582. [CrossRef]
11. Miranda, E.; Akkar, S.D. Generalized interstory drift spectrum. *J. Struct. Eng.* **2006**, *132*, 840–852. [CrossRef]
12. Munir, A.; Warnitchai, P. The cause of unproportionately large higher mode contributions in the inelastic seismic responses of high-rise core-wall buildings. *Earthq. Eng. Struct. Dyn.* **2012**, *41*, 2195–2214. [CrossRef]
13. Mehmood, T.; Warnitchai, P.; Suwansaya, P. Seismic evaluation of tall buildings using a simplified but accurate analysis procedure. *J. Earthq. Eng.* **2018**, *22*, 356–381. [CrossRef]
14. Najam, F.A.; Warnitchai, P. A modified response spectrum analysis procedure to determine nonlinear seismic demands of high-rise buildings with shear walls. *Struct. Des. Tall Spec. Build.* **2018**, *27*, e1409. [CrossRef]
15. Khan, F.R.; Sbarounis, J.A. Interaction of shear walls and frames. *J. Struct. Div.* **1964**, *90*, 285–335. [CrossRef]
16. Heidebrecht, A.C. Approximate analysis of tall wall-frame structures, B.S. Smith. *J. Struct. Div.* **1973**, *99*, 199–221. [CrossRef]
17. Smith, B.S.; Kuster, M.; Hoenderkamp, J.C.D. A generalized approach to the deflection analysis of braced frame, rigid frame, and coupled wall structures. *Can. J. Civ. Eng.* **1981**, *8*, 230–240. [CrossRef]
18. Smith, B.S.; Kuster, M.; Hoenderkamp, J.C.D. Generalized method for estimating drift in high-rise structures. *J. Struct. Eng.* **1984**, *110*, 1549–1562. [CrossRef]
19. Nollet, M.J.; Smith, B.S. Behavior of curtailed wall-frame structures. *J. Struct. Eng.* **1993**, *119*, 2835–2854. [CrossRef]
20. Miranda, E. Approximate seismic lateral deformation demands in multistory buildings. *J. Struct. Eng.* **1999**, *125*, 417–425. [CrossRef]
21. Miranda, E.; Reyes, C.J. Approximate lateral drift demands in multistory buildings with nonuniform stiffness. *J. Struct. Eng.* **2002**, *128*, 840–849. [CrossRef]
22. Miranda, E.; Taghavi, S. Approximate floor acceleration demands in multistory buildings. *J. Struct. Eng.* **2005**, *131*, 203–211. [CrossRef]
23. Reinoso, E.; Miranda, E. Estimation of floor acceleration demands in high-rise buildings during earthquakes. *Struct. Des. Tall Spec. Build.* **2005**, *14*, 107–130. [CrossRef]
24. Khaloo, A.R.; Khosravi, H. Multi-mode response of shear and flexural buildings to pulse-type ground motions in near-field earthquakes. *J. Earthq. Eng.* **2008**, *12*, 616–630. [CrossRef]

25. Xiong, H.; Zheng, Y.; Chen, J. A nonlinear computational model for regional seismic simulation of tall buildings. *Int. J. High-rise Build.* **2020**, *9*, 273–282. [CrossRef]
26. Kittiwuthikum, K. Effects of Foundation Flexibility on Dynamic Properties of Buildings in Bangkok. Ph.D. Thesis, Asian Institute of Technology, Khlong Nueng, Thailand, 2004. Available online: http://203.159.12.58/ait-thesis/detail.php?id=B08991 (accessed on 8 December 2021).
27. Singlumpong, T. Effects of Pile Foundation Flexibility on the Dynamic Characteristics of Multi-Story Buildings in Bangkok. Ph.D. Thesis, Asian Institute of Technology, Khlong Nueng, Thailand, 2006. Available online: http://203.159.12.58/ait-thesis/detail.php?id=B10088 (accessed on 8 December 2021).
28. Perform3D. *Nonlinear Analysis and Performance Assessment for 3D Structures Version 7*; Computers and Structures, Inc. (CSI): Berkeley, CA, USA, 2018.
29. Orakcal, K.; Wallace, J.W. Flexural modeling of reinforced concrete walls-model attributes, J.P. Conte. *Struct. J.* **2004**, *101*, 688–698.
30. Wallace, J.W. Behavior, design, and modeling of structural walls and coupling beams. Lessons from recent laboratory tests and earthquakes. *Int. J. Concr. Struct. Mater.* **2012**, *6*, 3–18. [CrossRef]
31. LATSBC. *The Structural Design of Tall and Special Buildings*; John Wiley & Sons Ltd.: Hoboken, NJ, USA, 2017.
32. Mander, J.B.; Priestley, M.J.N.; Park, R. Theoretical stress–strain model for confined concrete. *J. Struct. Eng.* **1988**, *114*, 1804–1826, 1827–1849. [CrossRef]
33. ACI Committee 318. *Building Code Requirements for Structural Concrete (ACI318M-11) and Commentary*; American Concrete Institute: Farmington Hills, MI, USA, 2011.
34. Paulay, T.; Priestley, M.J.N. *Seismic Design of Reinforced Concrete and Masonry Buildings*; John Wiley & Sons: Hoboken, NJ, USA, 1992.
35. Kappos, A.J.; Stylianidis, K.C.; Michailidis, C.N. Analytical models for brick masonry infilled R/C frames under lateral loading. *J. Earthq. Eng.* **1998**, *2*, 59–87. [CrossRef]
36. *ACI Code-530.1-11/ ASCE 6-11*; *Building Code Requirements and Specifications for Masonry*; Masonry Standards Joint Committee (MSJC): Boulder, CO, USA, 2011; pp. 602–611.
37. Suwansaya, P. Simplified Analysis Procedure to Determine the Nonlinear Seismic Demands of High-Rise Building with Reinforced Concrete Shear Walls. Ph.D. Thesis, Asian Institute of Technology (AIT), Khlong Nueng, Thailand, 2023.
38. Pandey, S.; Warnitchai, P.; Vasanthapragash, N.; Najam, F. Development of modal hysteretic model for the seismic response analysis of tall buildings with RC shear wall. In Proceedings of the 7th Asia Conference on Earthquake Engineering, Bangkok, Thailand, 22–25 November 2018.
39. Pandey, S. Development of Modal Hysteretic Model for the Seismic Response Analysis of Tall Buildings with RC Shear Wall. Master's Thesis, Department of Civil and Infrastructure Engineering. Asian Institute of Technology, Pathum Thani, Thailand, 2017.
40. McKenna, F. OpenSees: A framework for earthquake engineering simulation. *Comput. Sci. Eng.* **2011**, *13*, 58–66. [CrossRef]
41. Ancheta, T.D.; Darragh, R.B.; Stewart, J.P.; Seyhan, E.; Silva, W.J.; Chiou, B.S.; Wooddell, K.E.; Graves, R.W.; Kottke, A.R.; Boore, D.M.; et al. NGA-West2 database. *Earthq. Spectra* **2014**, *30*, 989–1005. [CrossRef]